

# **NMR Investigation of the Effect of Salts on Molecular Self-association**

Momo Jeufack Hervé

A Thesis submitted for the degree of Doctor of Philosophy

Department of Physics

University of Dortmund

January, 2006

---

# Contents

---

<b>1</b>	<b>General Introduction</b>	<b>1</b>
<b>2</b>	<b>Fundamentals of NMR</b>	<b>4</b>
2.1	Introduction . . . . .	4
2.2	Properties of Nuclear Spins . . . . .	5
2.3	Nuclei in a Static Magnetic Field . . . . .	6
2.3.1	The Vector Representation . . . . .	7
2.3.2	Radio Frequency Field and the Rotating Frame . . . . .	8
2.4	Internal Nuclear Interactions . . . . .	8
2.4.1	Dipolar interaction . . . . .	9
2.4.2	Quadrupole interaction . . . . .	10
2.4.3	Chemical shift . . . . .	11
2.4.4	J-coupling . . . . .	12
2.5	Dynamics of the Nuclear Spins . . . . .	12
2.5.1	Equation of Motion . . . . .	12
2.5.2	Nuclear Spin Relaxation . . . . .	14
2.6	Molecular Self-diffusion . . . . .	16

---

2.6.1	Pulsed Field Gradient NMR . . . . .	16
2.6.2	Gradient Calibration . . . . .	17
<b>3</b>	<b>Molecular Association and Hydrophobic Interaction</b>	<b>20</b>
3.1	Introduction . . . . .	20
3.2	Electrostatic Forces . . . . .	21
3.3	Van der Waals Forces . . . . .	22
3.4	The Hydrophobic Interactions . . . . .	23
3.4.1	Aqueous Solution . . . . .	24
3.4.2	Theory of Hydrophobic Interactions . . . . .	26
3.4.3	Amphiphile Solutions . . . . .	29
3.4.4	Factors Controlling the Micellar Structures . . . . .	31
3.4.5	Effect of Cosolute . . . . .	33
<b>4</b>	<b>Effect of Salts on Aqueous Solutions of Tertiary Butanol</b>	<b>35</b>
4.1	Introduction . . . . .	35
4.2	Structure of tert-Butanol . . . . .	36
4.3	Aqueous solution of tert-Butanol . . . . .	37
4.4	Theoretical approach . . . . .	38
4.4.1	Dipolar Relaxation Rate vs Pair Distribution Function	38
4.4.2	Self-association: the "A"-parameter . . . . .	41
4.5	Molecular Dynamics Simulations . . . . .	43
4.6	Experimental Strategies . . . . .	43
4.6.1	Relaxation Experiment . . . . .	43
4.6.2	Isotopic Dilution . . . . .	46
4.7	Results and discussions . . . . .	51
4.8	Conclusions . . . . .	57
<b>5</b>	<b>Effect of Salts on Model Biomembranes</b>	<b>59</b>
5.1	Introduction . . . . .	59
5.2	Model Biomembranes . . . . .	60
5.2.1	Lyotropic liquid crystalline phases . . . . .	61

---

5.2.2	Lipids and Bilayer Structure . . . . .	62
5.2.3	Magnetic Field Induced Orientation . . . . .	65
5.2.4	Material: the pentaethylene glycol monododecyl ether	67
5.2.5	Sample Preparation . . . . .	68
5.3	Deuterium Magnetic Resonance ( $^2\text{H}$ NMR) . . . . .	70
5.4	Experimental Considerations . . . . .	73
5.5	Results and Discussions . . . . .	73
5.6	Conclusion . . . . .	82
<b>6</b>	<b>Conclusion</b>	<b>84</b>
	<b>Bibliography</b>	<b>86</b>
	<b>Acknowledgements</b>	<b>97</b>

# CHAPTER 1

---

## General Introduction

---

In our dissertation, we study the influence of salt on the molecular self-association of nonpolar groups. Nonpolar entities include small organic molecules and large molecules (lipid, protein, DNA). The interactions between these molecules are at the origin of many biological processes such as protein folding, biological membrane formations, and condensation of DNA in cell nuclei.

Nonpolar regions appear to attract one another in water stronger than expected on the basis of thermodynamics [1–4]. This type of interaction, which is believed to be the driving force for self-association, is called the hydrophobic interaction. The origin of the effect is not clearly determined and some theoretical works have suggested that the rearrangement of the local water structure, the electrostatic fluctuation, the bridging bubbles and separation-induced phase transitions are some mechanisms which describe the hydrophobic attraction [5–8]

More specifically, we consider amphiphiles which contain both hydropho-

bic and hydrophilic groups. Amphiphilic molecules self-associate spontaneously in aqueous solution above the critical micelle concentration (cmc) into a variety of structures of well defined geometries, consisting of a hydrocarbon core with polar groups at the surface. The structural polymorphism ranges from spherical and cylindrical micelles to bilayer phases and more complex lyotropic crystalline phases (cubic phase). In biology for instance, the bilayer structures play a dominant role, since they form the biological membrane (lipid bilayer), the most common cellular structure in both animals and plants. Most of the time, the solution contains salts at different concentrations. A better understanding of the biological systems would be precious in many areas of science such as biochemistry, medicine, pharmaceutical and other fields. Model systems composed of artificially prepared amphiphilic materials and associated colloids serve a very useful purpose [9].

The morphology of the amphiphile aggregates depends on the nature of the amphiphiles, i.e. the size of the headgroup and the hydrophobic tail, but also on factors that influence the conformation of the hydrocarbon chain, the headgroup solvation and the interaction between neighboring head groups. Thus changing the amphiphiles or salt concentration or temperature affects not only the interactions between the aggregates but also the intermolecular forces within each aggregate, thereby modifying the self-assembled structures themselves [10–14].

Advanced applications of self-assembled systems include for example drug delivery [15] and the direct application of liquid crystalline phases as models for inorganic nanostructured materials such as mesoporous silica in catalysis [16].

We investigate the effect of salts (NaCl, NaBr and NaI) on the molecular forces, i.e the hydrophobic interaction, that is believed to determine the self-assembled structure such as biological membranes and allow some other biomolecules to adhere to them. To achieve our goal, we used NMR tools such as relaxation measurement, pulsed field gradient diffusion NMR and

deuterium NMR.

The first part of this dissertation provides the background for the experimental studies and theory for the molecular association. Thus chapter 2 is an introduction to basic concepts of NMR spectroscopy. In chapter 3 are discussed the molecular forces, with emphasis on the self-association and the concept of hydrophobic interaction. The second part consists of Chapter 4 describing the experimental approach to analyze the relatively simple system of tertiary butanol (TBA), considered as quasi hydrophobic substance, and chapter 5 introducing the biological membranes and the experiment on a model membrane, the pentaethylene glycol monododecyl ether ( $C_{12}E_5$ ). The last part, chapter 6 is a summary of the experimental findings, including the comparisons between the different studies and investigations reported in the literature.

---

# Fundamentals of NMR

---

## 2.1 Introduction

Though it was a scientific curiosity initially, the phenomenon of Nuclear Magnetic Resonance (NMR) has now evolved to a powerful analytical tool used in chemistry and physics for studying molecular structure and dynamics. Discovered initially by Purcell and Bloch shortly after the Second World War [17, 18], nuclear magnetic resonance spectroscopy studies the absorption of electromagnetic energy by inducement of transitions between spin states from lower to upper energy. Since the frequency of the emitted electromagnetic signals is determined by the energy difference of the states of the nuclei and the decay of the signal in time depends on the molecular environment of the nuclei, the NMR signals received by an rf probe can be analyzed to study the properties of the nuclei and their environment.

NMR has some advantages over other spectroscopic techniques, in the sense that it can non-invasively and non-destructively examine the physical



and chemical composition of materials. The method spans all the states of matter. Particularly, NMR methods can probe living systems in many levels of organization, ranging from the basic DNA, proteins, to biological membranes. Another category of application is the NMR imaging or magnetic resonance imaging, which is based on the same foundation as the classical NMR, is now widely used for clinical diagnostics, by supplying images of soft tissues of the body. Recently, the discovery that NMR can be used for developing quantum computers, with computing speed higher than the speed of the modern computers, has extended further the perspectives of nuclear magnetic resonance. It is obvious that the development of NMR spectroscopy has provided a wide field of spectacular applications not only in the field of chemistry but also extended to physics, biology, medicine and more.

In this chapter, we present a brief overview of the physical principles of NMR and the phenomenological treatment of an NMR experiment. The hardware of NMR spectrometers is widely discussed in the literature [19, 20], so we do not include any of those details for reasons that are evident.

## 2.2 Properties of Nuclear Spins

Certain atomic nuclei possess a property known as spin, which has a meaning only in the quantum mechanical framework, not discussed here. The property of nuclear spin is fundamental to the NMR phenomenon. A nucleus of spin quantum number  $I$  has a spin angular momentum  $J = \hbar I$ . To the angular momentum is associated a permanent spin magnetic moment  $\mu$  given by [21,22]

$$\mu = \gamma \hbar I, \tag{2.1}$$

where  $\gamma$  is the gyromagnetic ratio which is constant for any given nucleus and  $\hbar = h/2\pi$ ,  $h = 6.629 \times 10^{-34} \text{ J.s}$  being the Plank constant. The nuclei with  $I = 0$  possess no nuclear spin and therefore cannot exhibit nuclear magnetic resonance.

## 2.3 Nuclei in a Static Magnetic Field

When a strong external, static field  $\mathbf{B}_0 = (0, 0, B_0)$ , pointing in the  $z$ -direction, is applied, nuclei will adopt one of the two states: one has a higher energy level and the other has a lower energy level. The Hamiltonian  $H_Z$  or interaction energy of the nuclei is proportional to  $\mu$  and  $\mathbf{B}_0$  and is given by the expression

$$H_Z = -\mu\mathbf{B}_0, \quad (2.2)$$

whose eigenvalues are defined by

$$E_m = -\gamma\hbar m B_0, \quad (2.3)$$

where  $m$  are eigenvalues of the component of the angular momentum in the direction of  $\mathbf{B}_0$  and can take up  $2I + 1$  different values, defined as  $-I, -I + 1, \dots, I - 1, I$ . Each value of  $m$  defines an energy level and, in thermal equilibrium, the number of nuclei in the higher energy state is slightly less than the number of nuclei in the lower energy state. The energy level of stationary states are equally spaced with separation

$$\Delta E = \gamma\hbar B_0. \quad (2.4)$$

This equation shows that the energy difference is linearly proportional to the applied field. The distribution of spins between the lower energy state and the excited state is given by the Boltzmann relation

$$\frac{N_\alpha}{N_\beta} = e^{-\frac{\Delta E}{k_B T}} \approx 1 - \frac{\gamma\hbar B_0}{k_B T} \quad (2.5)$$

where  $N_\alpha$  and  $N_\beta$  are the numbers of spin in the lower and excited states,  $k_B = 1.3805 \times 10^{-23} \text{ J/K}$  is the Boltzmann constant and  $T$  is the temperature. A nucleus in the higher energy state can fall to the lower energy state by emitting a photon with energy equal to the energy difference between two states. A nucleus in the lower energy state can jump to the higher energy state by absorbing a photon with energy matching the energy difference between the two states. The magnetic resonance signal arises from transitions

between these energy levels induced by the absorption of a photon of frequency  $\nu$  or a quantum of energy

$$\Delta E = h\nu. \quad (2.6)$$

This energy is applied as an electromagnetic radiation, perpendicular to the static field, whose frequency must match that of the precessing nuclei or the Larmor frequency for the resonance condition to be satisfied. The Larmor frequency is given by the following expression:

$$\omega_0 = \gamma B_0. \quad (2.7)$$

After the irradiation of photons, the excess nuclei in the higher energy state will return to the lower energy state to recover the equilibrium, emitting photons or electromagnetic fields, which can be detected by an rf probe. These electromagnetic fields are known as NMR signal and their decay in time depend on the molecular environment of the observed nuclei.

### 2.3.1 The Vector Representation

For a collection of spins, the magnetic moments of the nuclei are randomly oriented in the absence of an external magnetic field and, therefore the resulting magnetic moment is zero. Once the magnetic field is applied, each individual magnetic moment must align itself either with or against the external field. These spin states are not equally populated, and the small population difference of nuclear spins can be represented as a collection of spins distributed randomly about the precessional cone and parallel to the  $z$  axis. The random distribution of individual magnetic moments about the cone generate no net magnetization in the transverse  $x$ - $y$  plane. Thus the picture of many similar magnetic moments can be reduced to one of a single bulk magnetization vector  $\mathbf{M}$  per unit volume, which is directly proportional in the high temperature approximation to the magnetic moments through Eq. (2.8) [23] :

$$\mathbf{M} = \frac{\Delta E}{2k_B T} N \mu_z \mathbf{e}_z \quad (2.8)$$

where  $N$  is the total number of spin per unit volume in the sample,  $T$  the temperature,  $k_B$  is the Boltzmann constant,  $e_z$  the unit vector along the  $z$ -axis and  $\mu_z = \gamma\hbar/2$ . This simplified picture is referred as the vector model of NMR and is used to describe the behavior of the spin in pulsed NMR experiments.

### 2.3.2 Radio Frequency Field and the Rotating Frame

The radio frequency field (rf), is an alternating field perpendicular to the static field  $\mathbf{B}_0$ . By convention, this field is called  $\mathbf{B}_1$  field. The concept of rotating frame is used to simplify the description of the nuclear spin motion when a rf pulse is applied. In the new frame, rotating about the  $z$ -axis,  $\mathbf{B}_1$  is stationary in the new transverse plane.

Usually, the manipulation of magnetic resonance phenomena is considered as motion in the rotating frame. Thus, the Hamiltonian of the rf pulse of general phase  $\phi$ , is written [20]:

$$H_1 = -\omega_1(I_x \cos \phi + I_y \sin \phi). \quad (2.9)$$

where  $\omega_1 = \gamma B_1/2$ . If the phase  $\phi$  takes the values 0, 90, 180, 270 degrees, they define in this order the  $x$ ,  $y$ ,  $-x$  and  $-y$  pulses.

A consequence of transformation into the rotating frame is that the magnetization appears to precess more slowly, at the difference ( $\Omega_0$ ) between the Larmor frequency ( $\omega_0$ ) and the rotating or transmitter frequency ( $\omega_r$ ),

$$\Omega_0 = (\omega_0 - \omega_r). \quad (2.10)$$

## 2.4 Internal Nuclear Interactions

In addition to the interaction of the nuclear spins with the applied external magnetic fields ( $\mathbf{B}_0$  and  $\mathbf{B}_1$ ), there exist other interactions among the magnetic moments within the spin-system. These interactions are referred as internal interaction.

### 2.4.1 Dipolar interaction

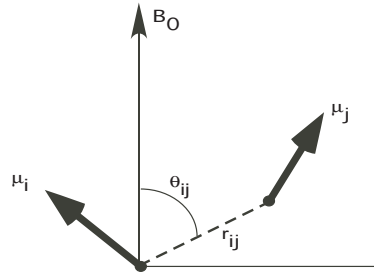


FIGURE 2.1: Geometry of the dipole-dipole interaction

The dipole-dipole interaction is due to a through space interaction of nuclear magnetic moments. The geometry of the interaction is shown on Fig. 2.1. The interaction Hamiltonian for dipolar coupled spins in the high-field approximation is [24]

$$H_{dd} = - \left( \frac{\mu_0}{4\pi} \right) \frac{\gamma_i \gamma_j \hbar}{r_{ij}^3} \frac{1}{2} \sum_{i < j} (3 \cos^2 \theta_{ij} - 1) [3 I_{iz} I_{jz} - \mathbf{I}_i \cdot \mathbf{I}_j], \quad (2.11)$$

where  $\mathbf{I}_i \cdot \mathbf{I}_j = I_{1x} \cdot I_{2x} + I_{1y} \cdot I_{2y} + I_{1z} \cdot I_{2z}$ ,  $r_{ij}$  is the distance between the two nuclei,  $\gamma_i$  and  $\gamma_j$  are the gyromagnetic ratio of the two spins,  $I_{mz}$  are angular momentum operators,  $\hbar$  is Planck's constant,  $\mu_0$  is the permittivity of free space and  $\theta_{ij}$  is the angle between the internuclear vector and the static magnetic field. The form of Eq. (2.11) is often referred to as the secular or truncated form or the dipole-dipole Hamiltonian. In solution, the dipole-dipole interaction is averaged to its isotropic value, zero, by molecular tumbling. This is not the case in liquid crystalline phases and solids where the interaction is a major cause of line broadening. There are two possible cases of dipolar coupling: homonuclear dipolar coupling, where spins  $I_i$  and  $I_j$  are the same species (e.g  $^1\text{H}$ ), and heteronuclear dipolar coupling, where spins  $I_i$  and  $I_j$  are different (e.g  $^1\text{H}$  and  $^{13}\text{C}$ ). In solution NMR, the measured dipolar coupling is [25]:

$$D_{ij} = - \left( \frac{\mu_0}{4\pi} \right) \gamma_i \gamma_j \hbar \left\langle \frac{(3 \cos^2 \theta_{ij} - 1)}{2r_{ij}^3} \right\rangle \quad (2.12)$$

where the angular brackets indicate the time and ensemble average of the dipolar Hamiltonian over all sampled orientations. Eq. (2.12) takes the value zero when all orientations are equally probable (in liquid for instance), but have a finite non-zero value when there is an anisotropic distribution of orientations relative to the static field direction.

### 2.4.2 Quadrupole interaction

The nuclear quadrupole interaction is the coupling of the nuclear quadrupole moment ( $Q_{ik}$ ) with the gradient of the electric field  $\nabla\mathbf{E} = (V_{ik})$  generated by the surrounding charges in the system. This behavior is a typical property of nuclei with spin  $> \frac{1}{2}$ .

The field gradient tensor ( $V_{ik}$ ) is usually defined in a molecule fixed coordinate system while the spin operators  $I_x, I_y, I_z$  are quantized along the laboratory frame. In the principal axes of the electric field gradient, the quadrupole Hamiltonian is simplified to [22]:

$$H_Q = \frac{eQ}{4I(2I-1)} [V_{zz}(3I_z^2 - \mathbf{I}^2) + (V_{xx} - V_{yy})(I_x^2 - I_y^2)], \quad (2.13)$$

where  $Q$  is the scalar quadrupole moment,  $e$  the elementary charge,  $\mathbf{I}$  is the total angular momentum operator, and  $V_{\alpha\alpha}$  are the second derivatives of the potential  $\mathbf{V}(x, y, z)$  produced at  $(x, y, z)$  by exterior charges. Usually two parameters are defined to characterize the gradient of the potential: the field gradient

$$eq = V_{zz}$$

and the asymmetric parameter

$$\eta = \frac{V_{xx} - V_{yy}}{V_{zz}}, \quad |V_{zz}| \geq |V_{yy}| \geq |V_{xx}|,$$

such that  $0 \leq \eta \leq 1$ . Both parameters are dictated by the dynamic process.

Given the total Hamiltonian  $H_Z + H_Q$ , the energy levels for the system can be computed. The allowed transitions are defined by  $\Delta m = \pm 1$ , where  $m = -I, \dots, I$  is the eigenvalue of  $I_z$ . The quadrupolar splitting  $\Delta\nu$  is a

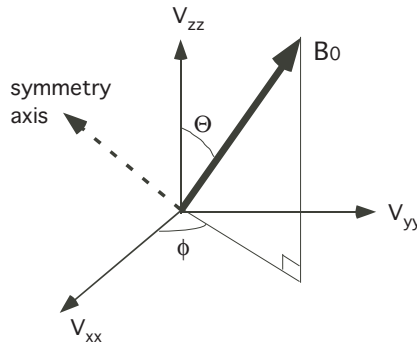


FIGURE 2.2: Geometry of the quadrupole interaction

function of the polar angles  $\Theta$  and  $\phi$  (see Fig. 2.2) that define the orientation of the principal axis system in the laboratory frame [26]. Thus,

$$\Delta\nu_Q(\Theta, \phi) = \frac{3 e^2 q Q}{2 h} \left( \frac{3 \cos^2 \Theta - 1}{2} + \frac{1}{2} \eta \sin^2 \Theta \cos 2\phi \right) \quad (2.14)$$

where the factor  $e^2 q Q / h$  is the quadrupole coupling constant. For axial symmetry such that  $V_{xx} = V_{yy}$ , that is  $\eta = 0$ , a simplified expression for the splitting is:

$$\Delta\nu_Q(\Theta) = \frac{3 e^2 q Q}{2 h} \left( \frac{3 \cos^2 \Theta - 1}{2} \right) \quad (2.15)$$

### 2.4.3 Chemical shift

The diamagnetic electrons surrounding the nuclei partially shield the applied magnetic field so that the local magnetic field at the site of the nucleus is different from  $B_0$  and both are related through the shielding tensor  $\sigma$  represented as a  $3 \times 3$  matrix. The local magnetic field is given by  $\sigma \mathbf{B}_0$ . The chemical shift effect describes the fact that the magnetic fields experienced by nuclei at two sites in the same molecule are different if the electronic environments are different. The internal Hamiltonian associated to this interaction for a given spin is defined by [27, 28]:

$$H_{cs} = \gamma \mathbf{I} \sigma \mathbf{B}_0. \quad (2.16)$$

### 2.4.4 J-coupling

The spin at one nucleus disturbs the electrons surrounding it. The resulting perturbation is transferred via the surrounding electrons of the molecule to electrons in the vicinity of the second nucleus. This effect is known as indirect spin-spin coupling. The interaction Hamiltonian is approximated by [24]:

$$H_J = \sum_{i < j} \mathbf{I}_i \mathbf{J}_{ij} \mathbf{I}_j \quad (2.17)$$

where  $\mathbf{J}_{ij}$  is the coupling tensor between spin  $i$  and  $j$  and has two contribution: an isotropic contribution and an anisotropic contribution.

## 2.5 Dynamics of the Nuclear Spins

### 2.5.1 Equation of Motion

Spin systems are statistical ensembles whose average state is frequently described by a density operator  $\rho(t)$  [20, 22, 24]. The density operator can be represented as a matrix with elements  $\langle n | \rho(t) | n' \rangle$ , where  $|n\rangle$  is a complete basis of states. Usually, the eigenstates of the nuclear spin Hamiltonian operator  $H$  are used as the basis, i.e.,  $H|n\rangle = E_n|n\rangle$ . Doing so, the diagonal elements of  $\rho(t)$  ( $n = n'$ ) are populations, i.e.,  $\langle n | \rho(t) | n \rangle$  is the probability of finding the system in the  $n$ th energy level. The off-diagonal elements ( $n \neq n'$ ) are called coherences if they are non-zero. At thermal equilibrium, there are no coherences, however coherences can be created by resonant rf pulses.

The expectation value of an operator  $\mathcal{O}$  for the spin state is given by

$$\langle \mathcal{O} \rangle = \text{tr}\{\mathcal{O} \cdot \rho(t)\}. \quad (2.18)$$

It follows particularly that the magnetization vector  $\mathbf{M}$  is related to the spin operator vector  $\mathbf{I}$  by

$$\mathbf{M} = N\gamma\hbar \text{tr}\{\mathbf{I} \cdot \rho(t)\} \quad (2.19)$$



where  $N$  is the number density of spins.

The change that the different nuclear interactions cause on the density operator is given by

$$\frac{d\rho(t)}{dt} = -i[H, \rho(t)]. \quad (2.20)$$

This equation, also known as the Liouville von Neumann equation, is derived from the time-dependent Schrödinger equation. The solution to this equation for a time-independent Hamiltonian is

$$\rho(t) = U(t)\rho(0)U^{-1}(t) \quad (2.21)$$

where  $\rho(0)$  is the density operator at time  $t = 0$  and the evolution operator is given by:

$$U(t) = \exp(-iHt) \quad (2.22)$$

The definition of  $U(t)$  assumes that the Hamiltonian is constant over the time period. Usually, this is not the case, for instance in multiple pulse experiment. The Hamiltonian changes when radio frequency pulses are applied from that which operates during the time gaps between pulses. For this reason, Eq. (2.22) is written

$$U(t) = \exp(-iH_n t_n) \dots \exp(-iH_1 t_1) \quad (2.23)$$

where the Hamiltonian which operates in the time  $t_n$  is  $H_n$ , and the factors are time-ordered (from right to left).

The density operator formalism is very convenient for the description of the dynamics of nuclear spins in NMR. The vector model, introduced earlier, is very useful for describing basic NMR experiments but unfortunately is not applicable to coupled spin systems. Specifically, in two-dimensional NMR many of the experiments are only of interest in coupled spin systems.

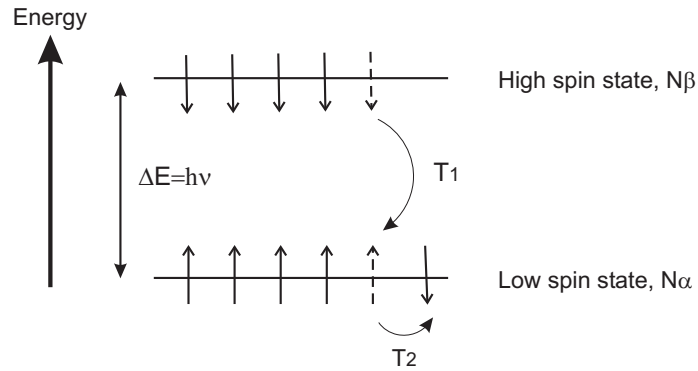


FIGURE 2.3: Resonance and Relaxation.  $T_1$  involves the exchange of Zeeman energy with the lattice,  $T_2$  processes do not alter the total Zeeman energy of the nuclear spin, i.e it conserves the energy of the spin state.  $N_\alpha$ ,  $N_\beta$  are populations of spin states.

## 2.5.2 Nuclear Spin Relaxation

Spin relaxation describes all phenomena, where a spin state  $\psi$  returns to the thermodynamic equilibrium state  $\psi_0$  due to a randomly fluctuating Hamiltonian. In NMR, these phenomena are of two different types. Each type depends upon different processes within the spin system. The first type takes place in the  $x$ - $y$  plane and is commonly known as the spin-spin or transversal relaxation, and is characterized by a time constant  $T_2$ . The transversal relaxation does not involve the exchange of spin energy with the lattice, but is concerned with the mutual exchange of spin energy via a flip-flop type mechanism, see Fig. 2.3. The second type of relaxation is the spin-lattice or longitudinal relaxation, occurs along the  $z$ -axis and is characterized by the time constant  $T_1$ .

The first phenomenological description of the motion of the net magnetization of isolated spins was done by Bloch [29]. The Bloch equations provide a simplified model for the behavior of a nuclear spin system after perturbation by a pulse. The Bloch equation may be written

$$\frac{dM_{x,y}}{dt} = \gamma(\mathbf{M} \times \mathbf{B})_{x,y} - \frac{M_{x,y}}{T_2} \quad (2.24)$$

$$\frac{dM_z}{dt} = \gamma(\mathbf{M} \times \mathbf{B})_z + \frac{M_0 - M_z}{T_1} \quad (2.25)$$

where  $M_0$  is the thermal equilibrium magnetization given by Eq. (2.8). These equations provide qualitative insights into the effects of relaxation on the NMR experiment and the relaxation rates can be measured experimentally. But it is worth emphasizing that nuclear spin relaxation is not a spontaneous process, it requires stimulation by a suitable fluctuating field to induce the necessary spin transition. Usually, a radio frequency field rotating at Larmor frequency is used to produce the transitions.

The Bloch formulation does not provide a microscopic explanation of the origin or magnitude of the relaxation time nor is it extensible to more complex coupled spin systems, for example, in dipolar-coupled two spin systems. In fact, as the molecules in the sample move due to the thermal motion, the magnitude and direction of the magnetic field exerted by one spin on the other changes. The fluctuating or time-dependent magnetic fields generated by the motion of neighboring molecules is the origin of the relaxation process. The fluctuation may be the dipole-dipole interaction, quadrupole interaction etc... and is considered as a small perturbation to the dominant Zeeman interaction. Usually a time-independent Hamiltonian is obtained by transformation to a frame rotating at the frequency  $\omega$  of the applied radio frequency. No such option is available for dealing with a randomly fluctuating Hamiltonian responsible for relaxation during the intervals between the pulses. Instead, the evolution of the spin density operator in the presence of random perturbation must be calculated either by numerical integration of Eq. (2.20), or by the formalism developed by Wangness and Bloch [30], and by Redfield [31].

## 2.6 Molecular Self-diffusion

The molecular self-diffusion can be defined as the translational motion of particles due to the changing interaction at the molecule vicinity (internal kinetic energy). The trajectory of any given molecule is irregular through the available space, Fig. 2.4. According to the geometry of the space, we can distinguish a free diffusion which takes place in an isotropic solution; and a restricted diffusion where the molecules diffuse within a confined space.

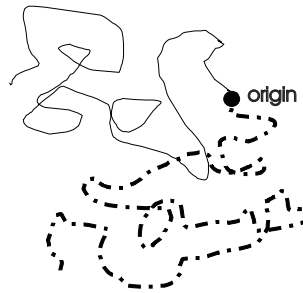


FIGURE 2.4: Chaotic trajectory: two particles, indicated by solid and dashed lines. The trajectories begin at the same origin yet follow different irregular paths.

### 2.6.1 Pulsed Field Gradient NMR

In pulsed field gradient (PFG) NMR, a magnetic field gradient is deliberately applied, making the NMR frequencies functions of position within the sample. The pulsed field gradient NMR self-diffusion experiment [32–34] is an important tool for investigations of diffusion processes in biological systems. The echo attenuation can be written in the general form [35] :

$$E(\mathbf{G}, \Delta) = \int \int \rho(\mathbf{r}) P(\mathbf{r}|\mathbf{r}', \Delta) \exp [i\gamma\delta\mathbf{G}\cdot(\mathbf{r} - \mathbf{r}')] dr' dr \quad (2.26)$$

where  $\rho(\mathbf{r})$  is the initial spin density,  $P(\mathbf{r}|\mathbf{r}', \Delta)$  the propagator is the conditional probability that a molecule initially at  $\mathbf{r}$  has moved to  $\mathbf{r}'$  after a time  $\Delta$ ,  $\delta$  and  $\mathbf{G}$  are the duration and magnitude of the gradient pulses.  $\Delta$  is also called the diffusion time. It is worth underlying that Eq. (2.26) is valid under

the short-gradient pulse approximation (SGP) since at the moment there is no universal model describing the echo decay as a function of the diffusion of molecules. Thus, the relationship between the signal attenuation and the diffusion constant is not so obvious to determine. The knowledge of the expression of  $P(\mathbf{r}|\mathbf{r}', \Delta)$  allows the integration of Eq. (2.26). For freely diffusing particles, the propagator is

$$P(\mathbf{r}|\mathbf{r}', \Delta) = \frac{1}{(4\pi Dt)^{3/2}} \exp \left[ -\frac{(\mathbf{r} - \mathbf{r}')^2}{4Dt} \right], \quad (2.27)$$

where  $D$  is the self-diffusion coefficient. For a system of arbitrary geometry, an analytical expression for  $P(\mathbf{r}|\mathbf{r}', \Delta)$  is not known but numerical methods can be used successfully [36].

## 2.6.2 Gradient Calibration

Nucleus	System	value of $D \times 10^9 / \text{m}^2 \text{s}^{-1}$
$^1\text{H}$	$\text{C}_6\text{H}_6$	$2.207 \pm 0.005$
	$\text{H}_2\text{O}$	$2.300 \pm 0.005$
	$\text{H}_2\text{O}/^2\text{H}_2\text{O}$ (trace)	$1.902 \pm 0.002$
	$\text{H}_2\text{O}/^2\text{H}_2\text{O}$ (10 mol.%)	$1.935 \pm 0.010$
$^{13}\text{C}$	$\text{C}_6\text{H}_6$	$2.207 \pm 0.007$

TABLE 2.1: Reference system for gradient calibration at 25°C. Adapted from ref [37]

It is very important to determine the gradient strength  $G$  as accurately as possible because there is a link in both precision of  $G$  and precision of  $D$ . In both pulsed gradient and static gradient NMR experiment the strength of the gradient required to achieve the results should be assigned. We just remind here that the static gradient is applied continuously during an experiment, and the magnitude of the gradient can be derived by the shape analysis of the echo [38], but this method has some drawbacks such as the deviation from the ideal geometry of the sample, which can distort the shape of the echo. It should be also possible to calculate the field gradient inside the

probe from the geometry of the gradient coil and the current through them. But this turns to be difficult and inaccurate particularly because the shape of the gradient coils might not be perfect, as the theoretical model. Usually the calibration is done indirectly by examining a sample of known  $D$  through the analysis of the echo decay of a PGSE experiment on a single component solution [39]. Some reference systems used in  $^1\text{H}$  and  $^{13}\text{C}$  NMR are given in Table 2.1. Even then this requires accurate temperature control.

For a gradient pulse applied, the amplitude of the echo is given by [32]

$$M(2\tau) = M(0) \exp \left[ -\frac{2\tau}{T_2} - (\gamma G \delta)^2 D \left( \Delta - \frac{\delta}{3} \right) \right], \quad (2.28)$$

where  $\tau$  is the time between the pulses,  $M(0)$  is the equilibrium magnetization,  $\delta$  and  $\Delta$  are the duration and the interval of the gradient pulses. The experimental dependence of the echo is normalized to a relative gradient

$$g = \frac{G}{G_{max}}, \quad (2.29)$$

where  $G_{max}$  is the maximum value of the pulsed gradient strength. The experimental dependence  $M(g)$  is fitted to a Gauss-function

$$M(g) = m_0 \exp \left( \frac{-g^2}{k^2} \right) \quad (2.30)$$

where  $m_0 = M(0) \exp \left( \frac{-2\tau}{T_2} \right)$  is constant and corresponds to the decay of the equilibrium magnetization  $M(0)$  with the relaxation time  $T_2$ , and  $k^2 = [(\gamma \delta)^2 D \left( \Delta - \frac{\delta}{3} \right) G_{max}^2]^{-1}$ . The experimental points and the fitted curve can be seen in Fig. 2.5.

The maximum gradient is calculated for a water sample at  $25^\circ\text{C}$  using the formula

$$G_{max} = \frac{1}{\sqrt{D_{cal} (\gamma \delta k)^2 \left( \Delta - \frac{\delta}{3} \right)}}, \quad (2.31)$$

where  $D_{cal} = 2.3 \times 10^{-9} \text{ m}^2/\text{s}$  is the diffusion coefficient of water at  $25^\circ$ .

For  $\gamma = 2.675 \times 10^8 \text{ s}^{-1}\text{T}^{-1}$ ,  $\delta = 3 \text{ ms}$ ,  $\Delta = 75.015 \text{ ms}$  and the fitting parameter  $k = 0.01048$ , Eq. (2.31) gives  $G_{max} = 9.15 \text{ T/m}$ . This value of  $G_{max}$  is

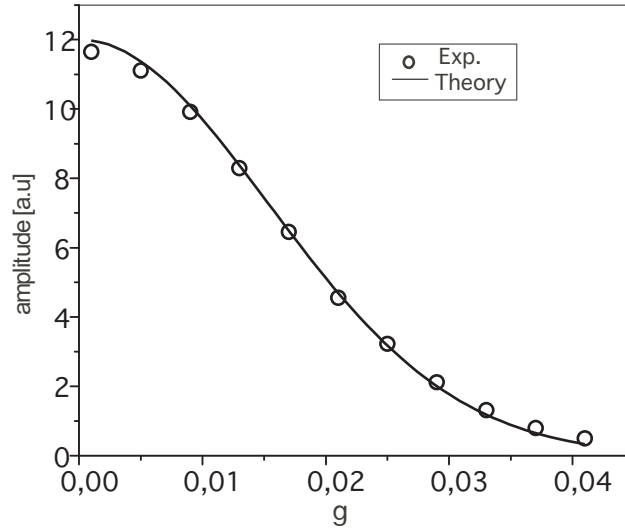


FIGURE 2.5: Profile of the diffusion experiment used for gradient calibration. The solid line is the best fit of the experimental data.

characteristic of the probehead used for our measurement. For each experiment, the diffusion coefficient can be obtained by applying the following formula:

$$D = \frac{1}{(\gamma \delta k_s)^2 \left(\Delta - \frac{\delta}{3}\right) G_{max}^2} \quad (2.32)$$

where  $k_s$  is the fitting parameter obtained for a given experimental conditions (samples, temperature).

---

# Molecular Association and Hydrophobic Interaction

---

## 3.1 Introduction

An understanding of the forces between molecules is the basic requirement for understanding the structure and properties of physical and biological systems. The forces act either within a molecule and they are called intramolecular forces, or they act between molecules and they are called intermolecular forces. A comprehensive treatment of the subject is found in elaborated textbooks [40–43]. Intramolecular forces are localized in the bonding region between atoms and are of short range in the sense that they act over bond distances of 0.1 – 0.2nm [42]. They are mostly covalent bond because they are limited to the interactions between atoms involved in molecular formation. In most of the system involving molecular association phenomena, the intramolecular forces are not of great interest, instead,



the intermolecular forces acting over distances greater than molecular bond dimensions are interesting. The intermolecular forces are responsible for aggregation/self-assembly and binding reaction in many biochemical processes [44]. The type of intermolecular binding forces operating between the molecules defines how different molecules should aggregate into one or another structure. The force between two molecules is defined by [40,41]:

$$F = -\frac{dw(r)}{dr} \quad (3.1)$$

where  $w(r)$  is the pair potential between two molecules or particles and correspond to the work done in bringing the two molecules from infinite separation to the separation  $r$ . The pair potential has various functional form for different types of forces.

The modification of the molecular microenvironment through addition of salts or other means has important consequences in structural integrity and dynamic of biological system. The intermolecular forces may be electrostatic in origin or may be derived from special interactions such as hydrophobic interaction.

## 3.2 Electrostatic Forces

Electrostatic forces arise from the coulombic interaction between charges and are fairly easy to understand. They are at the origin of the strong interaction among ions, among ions and polar molecules and among ions and non polar molecules, that is, they are involved when at least one formally charged species is present in the system. Ionic crystals (e.g. NaCl) are a good illustration of the electrostatic interaction; Fig. 3.1 shows the spacial arrangement of the charged species.

Electrostatic interactions are very important in molecular association either in inorganic system or biological systems such as nucleic acids and proteins. The potential between two ions is a function of their separation.

A hydrogen bond (H-bond) constitutes a particular case of electrostatic interactions where a hydrogen atom covalently bonded to an electronega-

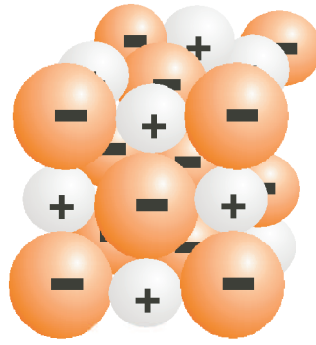


FIGURE 3.1: Ionic crystal of NaCl, composed of alternate positive and negative ions. The forces are attractive between unlike ions and repulsive between like ions. The overall interaction ensures the stability of the structure.

tive atom, such as oxygen, nitrogen or halogen (S, F), is able to approach another electronegative atom which may be within the same molecule or in a different molecule. The hydrogen bond is not unique to water and can occur also in nonpolar environments. They are particularly important in macromolecular and biological assemblies such as in proteins, linking different segments together inside the molecules and in nucleic acids, where they are responsible for the stability of the DNA molecule.

### 3.3 Van der Waals Forces

The van der Waals forces are separated in three types of atomic and molecular interactions: dispersion forces, induction forces and orientation forces. Each of which has its own characteristics, its own theoretical basis, and its own limitations [41]. The first two of the three are reasonably easy to understand because they are based on relatively straightforward electrostatic principles similar to those used for the much stronger coulombic interactions.

The dispersion interaction is very important in phenomena such as the properties of gases and liquids, the strengths of solid and the aggregation of particles in aqueous solutions, and the structures of condensed macro-

molecules such as proteins [41]. To understand the origin of dispersion interaction, we consider the interaction of two molecules neither of which has a permanent dipole moment. Although a molecule may possess no permanent dipole moment, its electrons are in continuous motion so that the electron density in a molecule oscillates continuously in time and space. Thus at any instant any molecule possesses an instantaneous electric dipole which fluctuates as the electron density fluctuates. This instantaneous dipole in one molecule induces an instantaneous dipole in a second molecule. The induced dipole in the second molecule and the inducing dipole in the first interact to produce an attractive energy called the dispersion energy. In other words, the dispersion energy is a result of the correlation between the electron density fluctuations in the two molecules. This force is the only contribution to the long range interaction of nonpolar molecules [40].

The induction contribution originates from the interaction between one molecule with a permanent dipole moment and a neutral molecule (i.e. non-polar molecule). In fact the electric field of the dipolar molecule distorts the electron charge distribution of the other molecule producing an induced dipole moment within it. This induced dipole then interacts with the nearby dipole to produce an attractive force. Inductive forces are simultaneously present with the electrostatic contribution in the case of the interaction of two polar molecules.

The orientation forces concern polar molecules with permanent dipole, and are generally significant only in systems involving very polar molecules [42].

### **3.4 The Hydrophobic Interactions**

The considerations of intermolecular forces in the paragraph above were more or less restricted to pure compounds that is only one type of attractive force is present. For a mixture of two or more components, more interactions occur simultaneously. Many of the characteristics of mixtures can be

explained in terms of the relative strength of the intermolecular forces between unlike pairs of molecules and those acting between the pure components. Thus the limited miscibility of water and liquid hydrocarbons such as tertiary butanol, is not an indication that molecules of water and tertiary butanol repel each other, but rather that they attract each other less strongly than water attracts another water molecule, and tertiary butanol attracts another tertiary butanol. The aspect of the molecular forces of interest is the self-association, occurring spontaneously in aqueous solution as a result of the attraction of like-like apolar groups, more specifically, the stability of these aggregates is believed to be due to the effective interaction between the apolar groups. This subject is usually discussed under the name hydrophobic effect or hydrophobic interaction. The literature on the subject is very wide [3, 4, 41, 45–48] and covers the anomalous thermodynamic properties of solutions [45], the formation of biological membranes and micelles [3], and the influence of solution environment on the structure of proteins [1].

The hypothesis for the theory of hydrophobic interaction were mainly built around the observations that, inert gases and simple hydrocarbons are barely soluble in liquid water and readily soluble in nonpolar solvents; the low solubility is coupled to the negative deviation of the standard entropy of solution.

### 3.4.1 Aqueous Solution

Aqueous solutions are defined as solutions in which water is the solvent. It is generally said that "*Water is life*". That is true in the sense that all known forms of life need water. Many biochemical processes require the presence of water [49]. Much has been written on the subject of water to explain its structure and the challenging properties [50].

The water molecule is a simple molecule consisting of two hydrogen atoms attached to an oxygen atom. Water has the chemical formula  $H_2O$ . For an isolated molecule, Fig. 3.2, the O-H bonds are at an angle of about

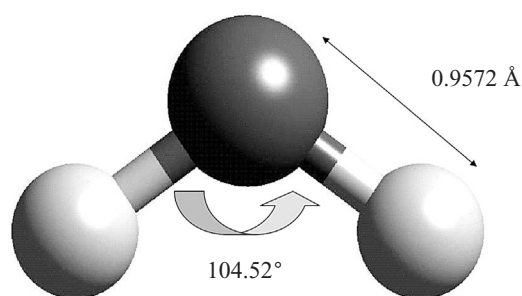


FIGURE 3.2: The average structure of a water molecule

105° between these bonds. This arrangement results in a polar molecule since there is a negative charge ( $\delta^-$ ) toward the oxygen end and a net positive charge ( $\delta^+$ ) at the hydrogen end. The polar nature of water and its ability to form hydrogen bonds make water a good solvent. Many authors [50–52] agree that liquid water structure consists of hydrogen bonds between molecule and emphasized a fundamental difference in properties between water and most other liquids. Among these properties, one can consider the anomalous thermodynamic behavior of aqueous solution.

The arrangements of water molecules must be altered when any solute is dissolved in it. If the solute particles are ionic or polar solute, strong bonds to water molecules can form, compensating by this fact the disruption of bonds existing in pure water, and making such solute easily soluble in water. Thus, water molecules reorient and partially neutralize charges (ionic charges) so that positive and negative charges do exist as separate entities, i.e. without forming ion pairs. The molecules at the first hydration shell (hydrating molecules) show much slower H-bond and reorientation dynamics than water molecules far away (bulk water) [53].

The H-bond compensation does not occur with nonpolar groups, making them barely soluble in water. Wiggins *et al.* [49] indicate that water molecules remain in a high energy state if they fail to arrange for the maximum number of hydrogen bonds with one another in the presence of nonpolar moieties. However the water molecules which are adjacent to the hy-

drophobic solute are in the higher energy state.

### 3.4.2 Theory of Hydrophobic Interactions

Many substances which form solids with strong intermolecular cohesion generally exhibit low solubility in all solvents. This is contrasted with hydrophobic substances defined as substances which are barely soluble in water but easily soluble in many nonpolar solvents. The limited miscibility of water and hydrophobic substances is known as the hydrophobic effect. In a macroscopic scale, the effect is summarized by the sentence: "Oil and water don't mix", as shown in Fig. 3.3. The behavior of nonpolar molecules which are unable to form hydrogen bond in aqueous solution is very fascinating. This behavior can not be explained only by the van der Waals interaction and the origin is not yet clearly understood.



FIGURE 3.3: Oil and water don't mix. Macroscopic illustration of the hydrophobic effect.

Frank *et al.* [51] in their investigation of the thermodynamic properties of aqueous solutions of hydrophobic substances gave the initial interpretation of the anomalous behavior of nonpolar solutes in aqueous solution, conferring the important role to the properties of water. This was later called the

hydrophobic effect or hydrophobic interaction or hydrophobic bond [52]. It was recognized that the modification of the water structure around nonpolar solute is accompanied by a loss of entropy, i.e hydrophobic units induce some order in the surrounding water. This effect is strengthened with increasing temperature and this is why the interaction is often viewed as an entropic phenomenon.

The loss in entropy is more pronounced for large molecules than for small molecules. The role of water in resolving protein conformation and denaturation was considered by Kauzmann [1] in his analysis of the forces stabilizing the native structure of proteins. He underlined the unique nature of the solvent medium in which the processes of life take place.

Biological structures are stabilized by a variety of forces. But, it is believed that the self-association between hydrocarbon chains or the hydrophobic interaction is the main stabilizing force [1,3].

At the moment there is no precise theory of hydrophobic interaction. While qualitative description of the hydrophobic effect is widely discussed in the literature, the lack of a formal theory of hydrophobic interaction makes a quantitative analysis very difficult. In a first approximation only ideal or pure hydrophobic substances are considered. The hydrophobic interaction exhibits many characteristics [48]. The hydrophobic interaction depends on the molecular size or hydrophobic cavity - which may consist of a molecular unit, large clusters or a combination of both. For a small hydrophobic cavity, the hydrogen bonded structure of water is maintained (four hydrogen bonds), although configured in a disordered manner. But in the case of large cavities, the hydrogen bond requirement of water can not be fully satisfied anymore ( $\leq 3$ ) in some region of space, because the dimension of the cluster doesn't allow the adjacent water molecules to maintain a complete H-bonds network with the surrounding liquid, see Fig. 3.4 for a pictorial description.

Many phenomenological descriptions do not consider this detailed aspect of the problem. Eriksson *et al.* [6] have developed a concept of mean

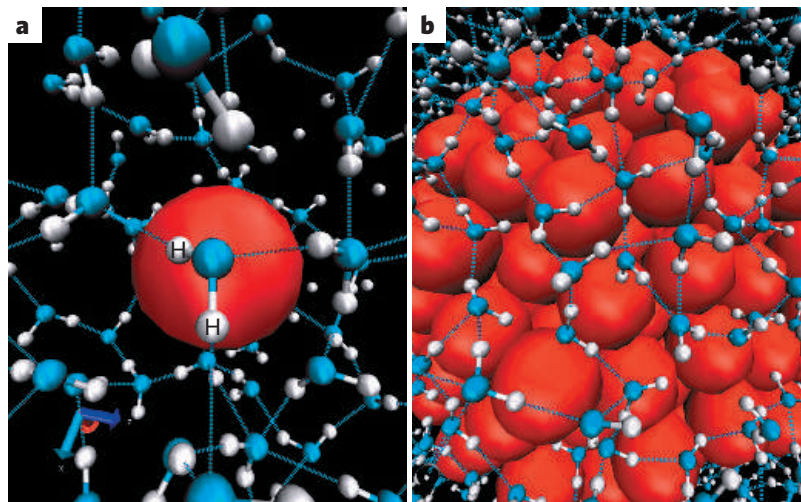


FIGURE 3.4: Configuration of liquid water molecules near hydrophobic cavities. a) The hydration of small cavity does not break hydrogen bonds. b) Solutes cluster together to form an hydrophobic unit with an extended surface. The dimension of the cluster doesn't allow the adjacent water molecules to maintain a complete H-bonds network with the surrounding liquid. Adapted from [48]

field theory of the hydrophobic attraction based on the notion of enhanced hydrogen bonding for the water molecules in the vicinity of hydrophobic surfaces. Their main conclusion suggests that a change in water structure may be at the origin of the observed hydrophobic interaction. Another explanation for the origin of the hydrophobic attraction relies on the electrostatic fluctuation [5]. In fact they propose that the hydrophobic attraction arises from electrostatic fluctuation between neutral bodies. Actually Ka Lum *et al.* [7] went further by considering two aspects of the hydrophobic attraction in terms of density fluctuations. In their analysis, they emphasized that the hydrophobic attraction of small apolar groups (alcohol) is not similar to those between large assemblies (proteins). Small apolar groups affect density fluctuations in water at small length scale, while large hydrophobic species can induce density fluctuations at large length scale. Some authors proposed that the hydrophobic attractions arise from the bridging of microscopic and submicroscopic bubbles adhering to the hydrophobic sur-



faces [8]. More importantly these bubbles exhibit a convex profile when there exists an attraction between the hydrophobic surfaces.

All these theories are defined in the context of ideal hydrophobic solutes, i.e objects which have no attractive interactions with the solvent particles, although real hydrophobic particles have some attraction for water (and vice versa), because of the omnipresence of van der Waals interactions [47].

However, pure hydrophobic or hydrophilic compounds are probably not very typical representatives of biophysical constituents. Another class of organic molecules, the so-called amphiphiles, containing polar and non-polar portions is usually found in biological systems.

### 3.4.3 Amphiphile Solutions

Amphiphiles are molecules consisting of two parts, one polar (hydrophilic, meaning it likes water) and the other one nonpolar (hydrophobic, meaning it avoids water) [3, 41, 54]. The hydrophilic part also is called the head group, it can be charged (anionic, cationic, zwitterionic) or polar (polyethylene chain, amine oxide). The hydrophobic or nonpolar portions, known also as the tail are usually hydrocarbons consisting of one or two linear chains as well as branched hydrocarbon chains. A typical structure of the amphiphilic molecules is given in Fig. 3.5. Molecule such as polyethylene glycol monododecyl ether have a head group made up of oxyethylene and a tail consisting of a long hydrocarbon unit.

In aqueous solution, amphiphiles can self-assemble into aggregates of different geometries generally called micelles. This class of substances is generally referred to as association or self-assembled aggregates. The micelles consist of a hydrocarbon core, with polar groups at the surface serving to maintain solubility in water. The size, shape, and basic structure of the associated structure are controlled by internal and external factors such as the chemical structure of the molecules, the solvent composition, the solute concentration, the temperature, etc...

Micelles can be small spheres or disks, oblate or prolate ellipsoids, or

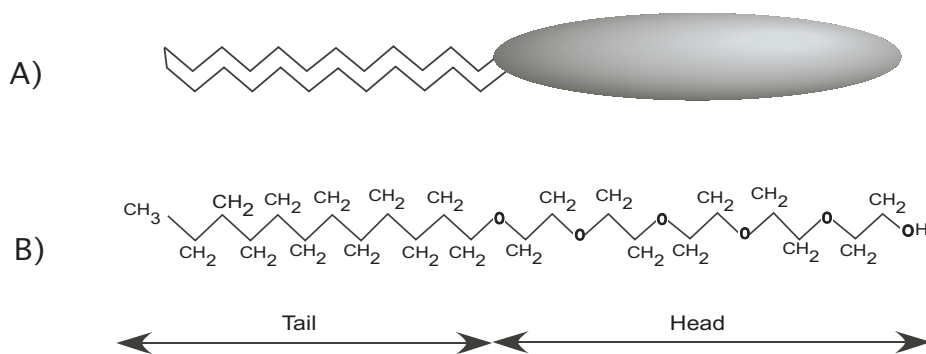


FIGURE 3.5: Schematic representation of an amphiphile: the pentaethylene glycol monododecyl ether ( $C_{12}E_5$ ). A) Simplified picture, B) Chemical structure

long cylinders. They can also be in the form of bilayers, that is, two parallel layers of amphiphile molecules with the polar groups facing out. Bilayer micelles often form more or less spherical vesicles (liposomes) with an internal solvent-filled cavity. The common features of these aggregates is that they possess well-defined hydrophobic domains in which the chains cluster into the core of the aggregates whilst the hydrophobic groups remain in contact with the solvent (water). The self-association is a spontaneous process resulting from the interaction between the individual solute molecules and the solvent medium. However, the aggregate starts only to form at a certain concentration of the solution called critical micelle concentration (cmc) and at a certain temperature called critical micelle temperature (cmt) [3], [41].

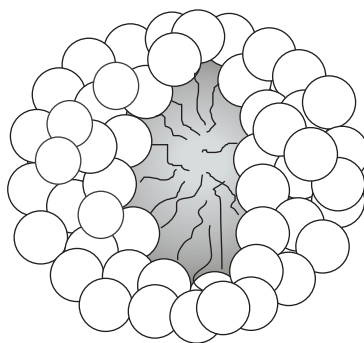


FIGURE 3.6: Schematic representation of a spherical micelle formed by aggregation of amphiphiles in aqueous solution. The micelle is opened to show the hydrocarbon core.

The basic types of biological amphiphiles are:

- Lipids which are structural components of biological membrane,
- Integral membrane proteins which, together with lipids serve as fundamental building blocks of biomembranes,
- Nucleic acids which are of two types: deoxyribonucleic acids (DNA) and ribonucleic acids (RNA).

At low concentration, amphiphiles may reduce effectively the surface tension. For this reason, they are also called *surfactant*, i.e. surface active agents, which refers to another feature of amphiphile substances. The surfactant self-assembly occurs in order to minimize the free energy of the solution. As a result they are very unstable, that is they are dynamic aggregates (making and breaking in a short time), able to rearrange (i.e. adopt a range of sizes and shapes ) in response to changing environmental conditions such as temperature. The most stable form of micelles is dictated by thermodynamic and geometric factors.

#### 3.4.4 Factors Controlling the Micellar Structures

Shape and size of micelles may be predetermined as the result of the competition of the hydrophobic interaction between the tails and the electrostatic repulsion between the head group. The geometric properties of the molecule and the head group charge influence the micellar shape. Now, it is recognized that the shape of micelles is strongly influenced by its tails also [55]. The micellar shape depends on the relative values of tail length ( $l$ ), effective head group area ( $a$ ) and the tail volume ( $v$ ) of the molecule, that is, the dimension of the amphiphile. A packing parameter, useful in determining a phase preference of an amphiphilic molecule, is defined by:

$$P = \frac{v}{al}. \quad (3.2)$$

The variables  $a$ ,  $v$  and  $l$  are all measurable [41], [3]. The possible packing geometries are listed in Table 3.1.






Packing shape	Packing parameter $P$	Structures formed
	$< 1/3$	spherical micelles
	$1/3 - 1/2$	cylindrical micelles
	$1/2 - 1$	vesicles, flexible bilayers
	$\sim 1$	lamellaes, planar bilayers
	$> 1$	inverse cylindrical and spherical micelles

TABLE 3.1: Packing parameter and the corresponding structures formed [41].

The thermodynamic aspect of self-aggregation is based on the change in free energy. An individual molecule in a solution has an interaction free energy (cohesive energy) which is the sum of its interactions with the surrounding molecules. The aggregate formation is regarded as changing the energy  $\mu_1$  (chemical potential) of a free monomer (molecule) of a system when an additional constituent of the same kind is introduced [41]. However, the change must be constant and equal to the change in the energy  $\mu_N$  of a molecule already in an aggregate of aggregation number  $N$  ( $N$  being also the number of constituent monomer molecules). This may be expressed as

$$\mu_N = \mu_N^0 + \frac{kT}{N} \ln \left( \frac{C_N}{N} \right) = \text{const}, \quad N = 1, 2, 3... \quad (3.3)$$

where  $\mu_N^0$  is the mean interaction free energy per molecule in aggregates of aggregation number  $N$ , and  $C_N$  is the concentration of molecules bound in aggregates of number  $N$  ( $N = 1$  corresponds to free molecules or amphiphiles).

However, the relevant physics lies in  $\mu_N^0$  and how it depends on  $N$ . It is denoted as:

$$\mu_N^0 = \mu_\infty^0 + \frac{\alpha kT}{NP} \quad (3.4)$$

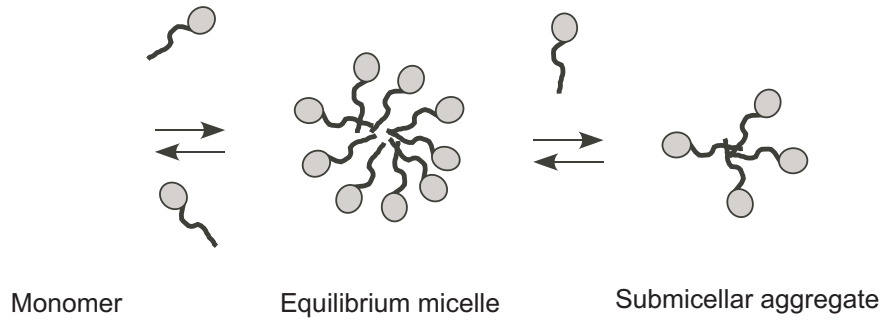


FIGURE 3.7: Amphiphiles are either present as un-aggregated monomers or are part of an aggregate consisting of  $N$  surfactant molecules. Micelles are dynamic aggregates, making and breaking in a short time, the residence time being estimated to be between  $10^{-5}$  and  $10^{-3}$ s [42].

where  $\alpha$  is a positive constant that dependent on the strength of the intermolecular interaction,  $P$  is the packing parameter,  $\mu_{\infty}^0$  is the energy of a molecule in an infinite aggregate. Stable aggregates form if  $\mu_N^0 - \mu_1^0 < 0$  for at least some value of  $N$ . So, the ability of amphiphiles to assemble into structures in which  $\mu_N^0$  reaches a minimum or constant value at some finite value of  $N$  limits the aggregate growth. This explains why the aggregates formed are not infinite (leading to phase separation) but of finite size (leading to micelle formations or micellization) and the critical micelle concentration ( $cmc$ ) is given by:

$$cmc \approx e^{-(\mu_1^0 - \mu_N^0)} \approx e^{-\alpha} \quad (3.5)$$

The  $cmc$  correspond to the concentration above which aggregates start to form in solution. The knowledge of how the molecular structure of the surfactant controls the shape and size of the resulting aggregate is useful in selecting molecules that would give desired structures such as bilayer vesicles, Fig. 3.6.

### 3.4.5 Effect of Cosolute

In addition to solvent (water) and solute (amphiphile), there exist also cosolute, traditionally considered as a second solute substance. An interesting

cosolute is salt. The salt can dissolve in water and acquire an ionic character. The ions then affect the solvent structure [10, 53] in addition to the specific interaction between the cosolute and the solute molecules. Regarding the solvent structure, some ions order water and they are called kosmotropes while other ions disorder water and they are called chaotropes.

The solubility of apolar particles such as noble gas is relatively lowered upon addition of salt [56]. The associated variation of the chemical potential is positive and is found to be proportional to the salt concentration [57].

---

# Effect of Salts on Aqueous Solutions of Tertiary Butanol

---

### 4.1 Introduction

The entropy of simple alcohols such as methanol increases less than expected for an ideal solution upon mixing with water. This effect has been assigned to the modification of the water structure, forming ice-like or clathrate-like structures around a solute molecule [1, 51]. Experimental and theoretical evidence suggested that hydrophobic portions of alcohol molecules in aqueous solution aggregate together [58, 59]. This behavior makes alcohol a good candidate to study the interaction between apolar groups. Tertiary butanol (TBA) is a simple amphiphile molecule and is used for the basic investigation of the hydrophobic interaction. These interactions are modified by the addition of salt and the mechanism remains poorly understood.

To understand efficiently the structural properties of the tert-Butanol/Water

system, and the effect salts can induce, it is important to know the structure of the basic components of the system.

## 4.2 Structure of tert-Butanol

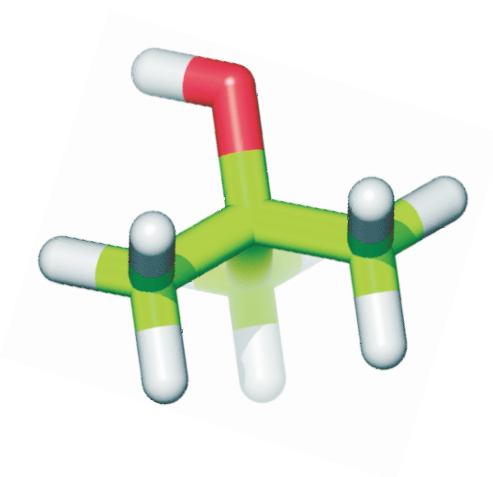


FIGURE 4.1: Three dimensional structure of a TBA molecule. The red shoulder indicates the position of the oxygen atom

Alcohols are important organic compounds that contain the hydroxyl (-OH) group. They are generally classified in three groups: primary, secondary and tertiary. The alcohol of interest, tert-Butanol, belongs to the third group. Tertiary alcohols have the hydroxyl group (-OH) attached to a carbon atom which has no hydrogen atom attached directly to it and is also bound to three carbons. Tert-Butanol has the chemical formula  $(\text{CH}_3)_3\text{COH}$ . The methyl group (- $\text{CH}_3$ ) form the hydrophobic head while the (-OH) group is the hydrophilic tail. This structure confers to the t-Butanol molecule an amphiphilic character.

The structure of liquid tert-Butanol is due to a mix of intermolecular interactions. A number of studies have attempted to propose a model for the structure. Neutron scattering [60] and molecular dynamics simulation [61] indicate that there exists a contact between the methyl groups of the alcohol as well as the hydrogen bonding interactions between the hydroxyl



group, and, that a significant number of polar to non-polar interactions are also present.

### 4.3 Aqueous solution of tert-Butanol

The interaction of water with alcohol is accompanied by a loss of entropy which is typical for hydrophobic system. This has led to a wide range of studies on this system and yet, understanding of the origin of this interaction still remains elusive. A number of studies on alcohol water mixture in atomic detail have been published, aimed at studying details of interaction and structural properties. For instance, study on TBA in water shows that besides the dominant non-polar contact, there are mixed polar-apolar contacts and there is no evidence for significant TBA-TBA hydrogen bonding [62,63]. The work of Soper *et al.* [64] involves neutron diffraction and indicates that water molecules form cages around methanol molecules in solution. Computer simulation has been used extensively to study the structure of tertiary butanol and the results claim little self-association of molecules for dilute solutions [65]. The investigation of Dixit *et al.* [66] have attributed the loss of entropy to an incomplete mixing water-alcohol solution at molecular level. More recently, Guo *et al.* [67] have performed x-ray emission spectroscopy whose result indicates that water molecules bridge methanol chains to form a ring structure containing 6 to 8 methanol molecules. Some experiments based on NMR, on different alcohols, have emphasized the dependence of the solubility (or hydrophobicity) of alcohol solutions on temperature, on concentration and on some cosolutes [11,13,68,69]. Moreover, the properties of aqueous solutions of ethanol are systematically influenced by salts [69]. This influence appears to be ordered in the Hofmeister series of aqueous solution [10].

Tertiary butanol-water solutions have been subjected to a particular attention. TBA is the largest monohydric alcohol fully miscible in water and is considered to be the most hydrophobic of the water-soluble alcohols [62].

Within the mixture exist different kinds of intermolecular interactions: the solute-solute, solute-solvent and solvent-solvent interactions. The temperature and concentration dependent studies on this system indicate that, the hydrophobic association (or solute-solute interaction) increases with dilution of the alcohol concentration and reaches a maximum at a concentration of about 2-3 mol % alcohol [11]. This has been the main motivation for the choice of this system for investigation of the hydrophobic interaction.

Upon addition of NaCl, the structure of the solute-solute interaction is affected as indicated by neutron scattering. Two coordination spheres are observed. Bowron *et al.* [12, 70] have inferred this structural change to the anion ( $\text{Cl}^-$ ), proposing that the anion might bridge a pair of TBA molecules. An investigation of the effect of different salts (NaBr, NaI) may yield additional information regarding either the location of the anion or the overall effect of salts on the association behavior of TBA molecules.

## 4.4 Theoretical approach

Information about the structure and translational motion can be obtained from spin-lattice relaxation measurements. Spin-lattice relaxation for interacting spins can be treated theoretically. The principles of the calculation of the spin-lattice relaxation emerged from the fundamental work of Bloembergen, Purcell and Pound [71], who considered the rates of transitions of the spins between energy levels, although more general formulations of the theory have been given by Wangsness and Bloch [30], and by Redfield [31]. The analysis is complicated by the fact that it is necessary to separate out the contribution due to the intramolecular and intermolecular dipole interactions.

### 4.4.1 Dipolar Relaxation Rate vs Pair Distribution Function

The mechanisms responsible for  $T_1$  relaxation are time-dependent interactions, such as the dipole-dipole interaction, the spin rotation interaction due

to the distribution of electrons in the rotating molecule, or to portions of the molecule; the chemical shift anisotropy interaction, due to the variability of the chemical shift as a function of the orientation of the molecule with respect to the static field; the scalar coupling interaction, due to fluctuations of the coupling constant  $J$ ; the quadrupolar relaxation (very large for nuclei with spin  $> \frac{1}{2}$ ), due to the changing direction of the electric field gradient at the nucleus; the paramagnetic interaction, due to the presence of unpaired electrons. Since all these interactions are of different strengths depending on a given situation, it follows that the relaxation rate will depend upon the precise mechanism responsible for relaxation.

In liquid solution, the dipole-dipole coupling is considered to be the main interaction responsible for nuclear relaxation for spin 1/2 ( $^1\text{H}$  only). An expression for the relaxation rate is determined by the time dependence of the magnetic dipole-dipole coupling. For two like spins, it is [72]

$$\begin{aligned} \frac{1}{T_1} = & 2\gamma^4\hbar^2 I(I+1)(\mu_0/4\pi)^2 & (4.1) \\ & \left\{ \int_0^\infty \left\langle \sum_j^N \frac{D_{0,1}[\Omega_{ij}(0)]}{r_{ij}^3(0)} * \frac{D_{0,1}[\Omega_{ij}(t)]}{r_{ij}^3(t)} \right\rangle e^{i\omega t} dt \right. \\ & \left. + 4 \int_0^\infty \left\langle \sum_j^N \frac{D_{0,2}[\Omega_{ij}(0)]}{r_{ij}^3(0)} * \frac{D_{0,2}[\Omega_{ij}(t)]}{r_{ij}^3(t)} \right\rangle e^{i2\omega t} dt \right\}, \end{aligned}$$

where  $D_{k,m}[\Omega]$  is the  $k, m$ -Wigner rotation matrix element of rank 2. The Eulerian angles  $\Omega(0)$  and  $\Omega(t)$  at time zero and time  $t$  specify the dipole-dipole vector relative to the laboratory fixed frame of a pair of spins and  $r_{ij}$  denotes their separation distance and  $\mu_0$  specifies the permittivity of free space. The expression of Eq. (4.1) for the relaxation rate consist of two contributions:

$$\frac{1}{T_1} = \frac{1}{T_{1,\text{intra}}} + \frac{1}{T_{1,\text{inter}}}, \quad (4.2)$$

an intramolecular part ( $1/T_{1,\text{intra}}$ ) generated by nuclei within the same molecule, and an intermolecular ( $1/T_{1,\text{inter}}$ ) contribution due to the nuclei in different molecules. This is illustrated in Fig 4.2.

The intramolecular contribution is basically due to molecular reorientations and conformational changes and has been used extensively to study

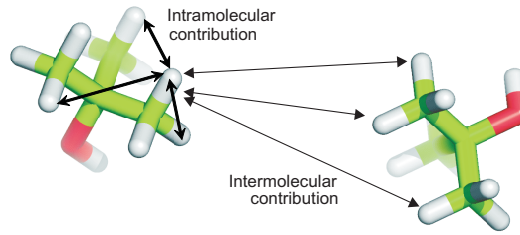


FIGURE 4.2: Cartoon showing the inter- and intramolecular dipolar couplings between nuclear spins of methyl groups

the reorientational motions, such as that of the H-H-vector in  $\text{CH}_3$ -groups in molecular liquids and crystals [73]. In the course of this work, however, we are particularly interested in the association of solute molecules, and will therefore focus on the intermolecular contribution.

For an isotropic fluid and in the extreme narrowing limit an expression of the intermolecular relaxation rate is obtained from Eq. (4.1) and is written [74,75]

$$\left(\frac{1}{T_1}\right)_{ij} = \frac{4}{3}\gamma^4\hbar^2 I(I+1)\kappa \int_0^\infty G(t) dt, \quad (4.3)$$

where  $G(t)$  is the dipole-dipole time correlation function,  $\kappa = 3/2$  for homonuclear interactions and  $\kappa = 1$  for heteronuclear interactions.  $G(t)$  is defined by [72,76]

$$G(t) = \left\langle \sum_j r_{ij}^{-3}(0) r_{ij}^{-3}(t) P_2[\cos \theta_{ij}(t)] \right\rangle, \quad (4.4)$$

where  $r_{ij}$  is the distance between the spins  $i$  and  $j$  and  $\cos \theta_{ij}(t)$  is the angle between the vector joining spins  $i$  and  $j$  at time 0 and time  $t$ .  $P_2$  is the second Legendre polynomial.

The integral of  $G(t)$  of Eq. (4.3) defines the spectral density at  $\omega = 0$  which is a function of the randomly modulated local interaction. To integrate it, we should separate the correlation function into an  $r^{-6}$ -prefactor, which is sensitive to the structure of the liquid (average intermolecular spin-spin distances) and a correlation time  $\tau_c$ , which is obtained as the time-integral of the normalized correlation function, and which is sensitive to

the mobility of the molecules in the liquid,

$$\int_0^{\infty} G(t) dt = \left\langle \sum_j r_{ij}^{-6}(0) \right\rangle \tau_c . \quad (4.5)$$

From the definition of the dipole-dipole correlation function in Eq. (4.4) it follows directly that the relaxation time  $T_1$  is affected by both, reorientational and translational motions. It is obvious that it also depends strongly on the average distance between the spins and hence is sensitive to changing inter- and intramolecular pair distribution functions [77,78]. In addition, the  $r^{-6}$ -weighting introduces a particular sensitivity to changes occurring at short distances.

The structure of the liquid can be expressed in terms of the intermolecular site-site pair correlation function  $g_{ij}(r)$ , describing the probability of finding a second atom of type  $j$  in a distance  $r$  from a reference site of type  $i$  according to [79]

$$g_{ij}(r) = \frac{1}{N_i \rho_j} \left\langle \sum_{k=1}^{N_i} \sum_{l=1}^{N_j} \delta(\vec{r} - \vec{r}_{kl}) \right\rangle , \quad (4.6)$$

where  $\rho_j$  is the number density of atoms of type  $j$ . The prefactor of the intermolecular dipole-dipole correlation function is hence related to the pair distribution function via an  $r^{-6}$  integral of the pair correlation function

$$\left\langle \sum_j r_{ij}^{-6}(0) \right\rangle = \rho_j \int_0^{\infty} r^{-6} g_{ij}(r) 4\pi r^2 dr . \quad (4.7)$$

Since the process of enhanced association in a molecular solution is equivalent with an increase of the nearest neighbor peak in the radial distribution function, Eq. (4.7) establishes a quantitative relationship between the degree of intermolecular association and the intramolecular dipolar nuclear magnetic relaxation rate.

#### 4.4.2 Self-association: the "A"-parameter

As a measure of the degree of intermolecular association, Hertz and co-workers [77,78,80] introduced a so-called association parameter "A", which

is a weighted integral of the pair correlation function of the nuclei contributing to the dipolar relaxation process (in the present case  $^1\text{H}$  nuclei in TBA-d1) and is defined as [81]:

$$A = \frac{1}{2} \frac{\gamma^4 \hbar^2}{a^4} \left( \frac{\mu_0}{4\pi} \right)^2 \int_0^\infty \left( \frac{a}{r} \right)^6 g_{HH}(r) 4\pi r^2 dr, \quad (4.8)$$

where the distance  $a$  is introduced to represent the "closest approach distance of the interacting nuclei",  $g_{HH}$  stands for the proton-proton pair correlation function. A useful approximation relates this distance  $a$ , the dipole-dipole correlation time  $\tau_{\text{inter}}$  and the self-diffusion coefficient  $D$  through

$$\tau_{\text{inter}} = \frac{a^2}{3D}. \quad (4.9)$$

The  $A$ -parameter is a useful measure in the sense that it is directly related to the solvent mediated attractive or repulsive interactions between solute molecules through the sharpness, or peak-height, of the pair correlation function. The relative change of the local concentration of the observed molecules is identified by the relative change in the  $A$ -parameter: as  $g_{HH}(r)$  becomes sharper when the density of the next neighbor atoms around the reference atom increases, the  $A$ -parameter increases. Using the definitions of Eq. (4.8) and Eq. (4.9), " $A$ " is given in terms of NMR measurable quantities [81,82]:

$$A = \frac{1}{T_{1,\text{inter}}} \cdot \frac{D}{\rho_{\text{H}}} \quad (4.10)$$

where  $D$  is the self-diffusion coefficient of the solute molecules and  $\rho_{\text{H}}$  is the number density of the  $^1\text{H}$ -nuclei in the system. Making use of the concentration dependence outlined in Eq. (4.10), the aggregation behavior of solvent molecules should be determined [11,13]: an enhanced association is identified by an increasing  $A$ -parameter, whereas a de-association corresponds to a decrease. In the present case, where we vary the salt concentration, we measure the change of the  $A$ -parameter with the salt concentration.

## 4.5 Molecular Dynamics Simulations

Molecular dynamics (MD) simulations provide information about the dynamics of the molecules. Correlation functions can be derived, which describe the tendency of the molecules to form clusters.

The pair correlation function  $g(r)$  provides a measure of local spatial ordering in a solution:  $g(r)$  is the probability of finding a second solute molecule in a distance  $r$  from a reference solute molecule. More details on the simulation parameters are given in a paper submitted in the course of this work [83].

## 4.6 Experimental Strategies

### 4.6.1 Relaxation Experiment

In a relaxation experiment each data acquisition consists of an excitation and detection of magnetization. The most commonly applied method for  $T_1$  determination is the inversion recovery method combined with Fourier transform (IRFT). The experiment is a simple two pulses sequence, Fig. 4.3. This experiment can be described in terms of a density operator and an expression for the transverse magnetization derived.

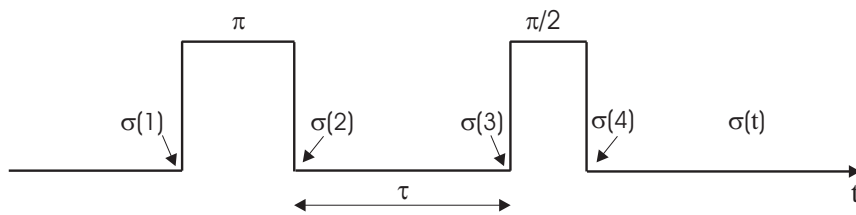


FIGURE 4.3: Inversion recovery pulse sequence for  $T_1$  measurement.  $\sigma$  is the density operator.

The total Hamiltonian of the system in the rotating frame is given by:

$$H = \hbar\Omega_0 I_z + \hbar\omega_1 I_x. \quad (4.11)$$

where  $\Omega_0$  is the rotating frame frequency defined by Eq. (2.10). Before the first pulse, the spin density operator in terms of angular momentum operators corresponds to

$$\sigma(1) = \frac{1}{2}\mathbb{1} + bI_z \quad (4.12)$$

where  $b = \gamma\hbar B_0/2k_B T$  and  $\mathbb{1}$  is the identity operator. The first pulse  $\pi_x$  generates an inverted population distribution,

$$\sigma(2) = \frac{1}{2}\mathbb{1} - bI_z. \quad (4.13)$$

The net magnetization placed along the  $-z$ -axis will gradually return to its equilibrium position along the  $+z$ -axis during the time interval  $\tau$  at a rate dictated by  $T_1$ . After a free evolution with  $T_1$  relaxation,

$$\sigma(3) = \frac{1}{2}\mathbb{1} + b[1 - 2\exp(-\tau/T_1)]I_z; \quad (4.14)$$

The second pulse  $(\pi/2)_x$ , converts the population difference into coherence

$$\sigma(4) = \frac{1}{2}\mathbb{1} - b[1 - 2\exp(-\tau/T_1)]I_y; \quad (4.15)$$

A free evolution of the coherence with  $T_2$  relaxation transforms the density operator to

$$\sigma(t) = \frac{1}{2}\mathbb{1} + b(I_x \sin \Omega_0 t - I_y \cos \Omega_0 t)[1 - 2\exp(-\tau/T_1)]\exp(-t/T_2). \quad (4.16)$$

Using Eq. (2.19), the complex transverse magnetization  $M_x + iM_y = M^+$  can explicitly be written in the form :

$$M^+(t) = \frac{N\gamma^2\hbar^2 B_0}{4k_B T}(\sin \Omega_0 t - i \cos \Omega_0 t)[1 - 2\exp(-\tau/T_1)]\exp(-t/T_2). \quad (4.17)$$

The receiver introduces a phase shift  $\varphi$  and the magnetization with the mixed phase is written :

$$\begin{aligned} M^+(t) &= \frac{N\gamma^2\hbar^2 B_0}{4k_B T}(\sin(\Omega_0 t + \varphi) - i \cos(\Omega_0 t + \varphi)) \\ &\times [1 - 2\exp(-\tau/T_1)]\exp(-t/T_2). \end{aligned} \quad (4.18)$$

In the frequency domain, the magnetization  $M^+(\omega)$  is the Fourier transform of  $M^+(t)$ :

$$M^+(\omega) = \int_{-\infty}^{+\infty} M^+(t)e^{-i\omega t} dt. \quad (4.19)$$



The complex spectrum of transverse magnetization is then given by:

$$M^+(\omega) = iM_0(1 - 2e^{-\tau/T_1}) \times \frac{(\omega - \Omega_0) \sin \varphi + \lambda \cos \varphi - i[(\omega - \Omega_0) \cos \varphi - \lambda \sin \varphi]}{\lambda^2 + (\omega - \Omega_0)^2} \quad (4.20)$$

where  $\lambda = 1/T_2$ . The amplitude of the spectrum is defined by:

$$A_0(\tau) = M_0(1 - 2e^{-\tau/T_1}). \quad (4.21)$$

The real part of the complex spectrum is a Lorentzian mixed phase. The intensity  $I(\tau)$  of the spectrum is proportional to the amplitude  $A_0(\tau)$ ,

$$I(\tau) = I_o(1 - 2e^{-\tau/T_1}) \propto A_0(\tau). \quad (4.22)$$

This expression is valid for ideal experimental conditions. In practice, the inhomogeneity of the rf field, the resonance frequency offset, the inaccuracies in  $\pi$ -pulse calibration, which causes imperfect initial inversion, lead to errors in the resulting  $T_1$ . The modified function [84,85],

$$I(\tau) = A + B e^{-\tau/T_1}, \quad (4.23)$$

is preferred to overcome these sources of errors.  $A$ ,  $B$  and  $T_1$  are free adjustable parameters determined by a non-linear fit of the experimental data [86], see Fig. 4.4.

Usually enough time ( $> 5 T_1$ ) is allowed between acquisitions that the equilibrium spin temperature is fully restored. Repeating the experiment with increasing values of the pulse delay  $\tau$  allows one to follow the relaxation of the spin.

After processing the spectra, each individual peak is integrated for maximum accuracy in the relaxation curve. The starting and stopping points must be chosen carefully. Baseline artifacts can affect significantly the reliability of integral values. Accurate integral values are obtained when the baseline is relatively flat. Since NMR peaks approach the baseline only very gradually, the integration limits should be placed a distance from the peak, in order to insure that as much as possible of the peak is included.

Each  $T_1$  value reported is the average obtained from the analysis of three sets of relaxation data with two scans per spectrum. The pulse phases were 0 for the  $\pi$ -pulse, and alternated between 0 and 180 for the  $\pi/2$ -pulse.

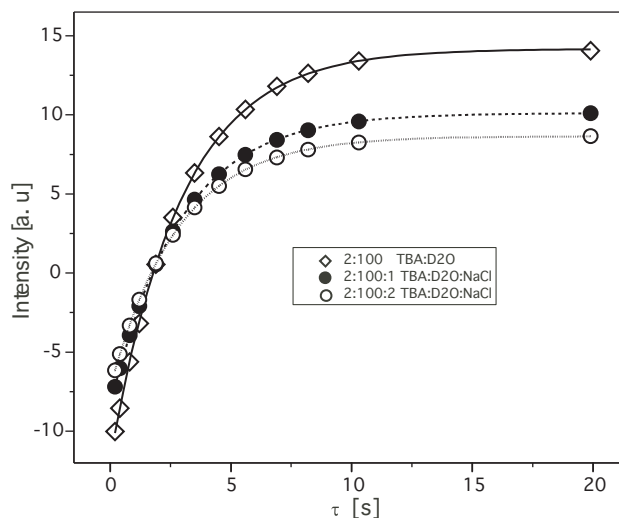


FIGURE 4.4: Non-linear fit of the data for an inversion recovery experiment

## 4.6.2 Isotopic Dilution

The observed relaxation rates depend on inter- as well as intra-molecular correlation functions. To extract the intermolecular rates, which are sensitive to the solute-solute association, we used the method of isotopic dilution [87].

Since we are interested only in the hydrophobic methyl-protons, we deuterated the water and the hydroxyl group of the TBA. Isotopic dilution was performed by mixing  $(\text{CH}_3)_3\text{COD}$  (TBA-d1)<sup>1</sup> with its perdeuterated analog  $(\text{CD}_3)_3\text{COD}$  (TBA-d10). We parameterize the dilution with the mole fraction

$$x_{\text{H}} = \frac{[\text{TBA-d1}]}{[\text{TBA-d1}] + [\text{TBA-d10}]} \quad (4.24)$$

The anhydrous TBA-d1 (99%) was purchased from Cambridge Isotope laboratories, the TBA-d10 (99%) from Isotec. The solvent  $\text{D}_2\text{O}$  with the purity 99.96% was obtained from Merck KGaA. The solution was prepared by

<sup>1</sup>Using  $(\text{CH}_3)_3\text{COD}$  instead of  $(\text{CH}_3)_3\text{COH}$ , serves to eliminate any intra or inter contribution from t-butanol hydroxyl protons. We are using  $\text{D}_2\text{O}$  as solvent instead of  $\text{H}_2\text{O}$  in order to "shutdown" the  $^1\text{H}-^1\text{H}$  dipole-dipole interaction with water molecules

measuring the appropriate amount of each compound with a micropipette, and by weighing corresponding amount of salts (NaCl, NaBr, NaI).

The TBA and water molecules are in the stoichiometric ratio  $k$  :

$$\frac{n_b}{n_D} = k \Rightarrow n_b = k n_D \quad (4.25)$$

where  $n_b$  and  $n_D$  denote the total number of moles of TBA and of D<sub>2</sub>O respectively. It follows the relation for the mole fraction  $x_b$  and  $x_D$ :

$$x_D = \frac{1}{1+k} \quad (4.26)$$

$$x_b = \frac{k}{1+k} \quad (4.27)$$

For a given volume  $V_D$  of D<sub>2</sub>O, the volume of TBA-d1 ( $V_{TBA}$ ) and of TBA-d10 ( $V_{d10}$ ) needed to be in the proportion  $k$  are given by:

$$V_{TBA} = k x_H \frac{\rho_D}{\rho_{TBA}} \frac{M_{TBA}}{M_D} V_D \quad (4.28)$$

$$V_{d10} = k(1-x_H) \frac{\rho_D}{\rho_{d10}} \frac{M_{d10}}{M_D} V_D, \quad (4.29)$$

where  $M_{TBA} = 75.11\text{g/mol}$  and  $\rho_{TBA} = 0.797\text{g/ml}$ ,  $M_D = 20.3\text{g/mol}$  and  $\rho_D = 1.107\text{g/ml}$ ,  $M_{d10} = 84.18\text{g/mol}$  and  $\rho_{d10} = 0.893\text{g/ml}$

The salt concentration is calculated with respect to that of the solvent. If the salt and D<sub>2</sub>O are in the stoichiometric ratio  $k_1$ ,

$$k_1 = \frac{n_{sc}}{n_D}, \quad (4.30)$$

then the quantity of salt required is given by :

$$m_s = k_1 \rho_D \frac{M_s}{M_D} V_D. \quad (4.31)$$

The degassing process was done carefully by the usual freeze-pump-thaw technique, repeated several times until no gas bubbles developed from the solution. If by any means the samples were not totally degassed, then the influence of the oxygen will lead to wrong results since the variation of the proton concentration is very small during the isotopic dilution.

The temperature control is a very important part of the isotopic dilution experiment. Although a temperature controller is built to regulate the flow

samples	$x_H$	$V_D$	$V_{TBA}$	$V_{d10}$
S1	1.00	490	51.0	0.0
S2	0.75	490	38.3	12.8
S3	0.50	490	25.5	25.5
S4	0.25	490	12.8	38.3

TABLE 4.1: Composition of the samples 2:100:0 TBA:D<sub>2</sub>O:NaCl used for the isotopic dilution experiment. The volumes are in microliters.

rate of hot or cool air in the probe, the temperature set from the electronic console generally doesn't correspond to the temperature read at the sample location. The read temperature is measured by introducing a thermocouple at the sample location inside the probehead. In fact a given flow rate corresponds to a heating profile as shown in Fig. 4.5. This type of calibration allows us to measure always at the desired temperature, which is 25°C in our measurement. Only with a good temperature calibration, results measured at different time periods and on different samples can be compared successfully.

The basic assumption of the isotopic dilution procedure is that the relaxation rate is given by the sum of an intramolecular term, which is independent of the dilution, and an intermolecular term, which is proportional to the concentration of the corresponding molecular species.

$$\frac{1}{T_1} = \frac{1}{T_{1,0}} + \frac{1}{T_{1,\text{intra}}} + \frac{x_H}{T'_{1,\text{inter}}} + \frac{(1-x_H)}{T''_{1,\text{inter}}} \quad (4.32)$$

Here,  $T_{1,\text{intra}}$  denotes the intramolecular contribution from protons within the methyl groups of the same molecule as the one being measured,  $T'_{1,\text{inter}}$  and  $T''_{1,\text{inter}}$  the intermolecular contributions between TBA-TBA and TBA-(TBA-d10) molecules respectively, and  $T_{1,0}$  all other terms, such as paramagnetic relaxation and interaction with other molecules such as D<sub>2</sub>O. The contribution of the deuterated molecules can be taken as proportional to

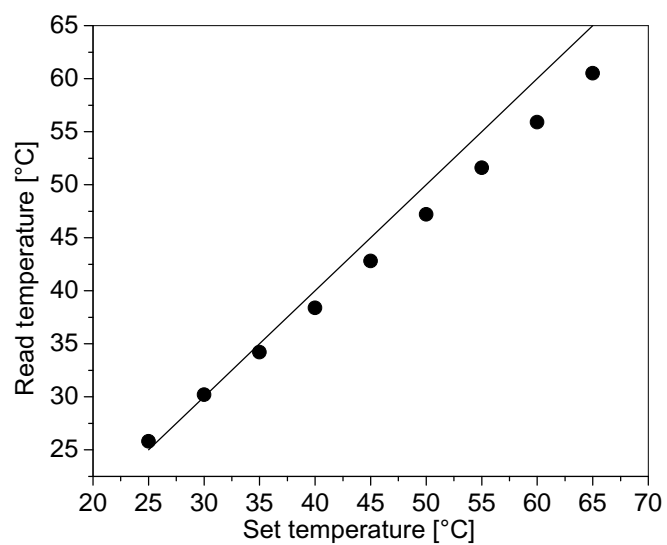


FIGURE 4.5: Temperature calibration. The temperature set does not always correspond to the temperature at the sample location and the solid line represents the ideal case of perfect correspondence. In our case we manage to have a flow such that the set temperature correspond to the read temperature for the given gas flow rate.

that of the protonated molecules, with a reduction factor [21]<sup>2</sup>

$$\frac{1/T''_{1,\text{inter}}}{1/T'_{1,\text{inter}}} = \frac{2 \gamma_D^2 I_D(I_D + 1)}{3 \gamma_H^2 I_H(I_H + 1)} = \alpha = 0.042. \quad (4.33)$$

The observed relaxation rate becomes therefore

$$\frac{1}{T_1} = \frac{1}{T_{1,0}} + \frac{1}{T_{1,\text{intra}}} + \frac{1}{T_{1,\text{inter}}} [(1 - \alpha)x_H + \alpha], \quad (4.34)$$

where  $T_{1,\text{inter}}$  is the intermolecular contributions between different TBA molecules.

To extract the intermolecular term, we measured the relaxation rate as a function of the isotopic dilution and fitted the measured data points to Eq. (4.34). Figure 4.6 is an illustration of the procedure. The quantity  $\frac{1}{T_{1,0}} + \frac{1}{T_{1,\text{intra}}}$  of Eq. (4.34) is the intercept with the  $y$  axis and is considered as the intramolecular contribution in the analysis.

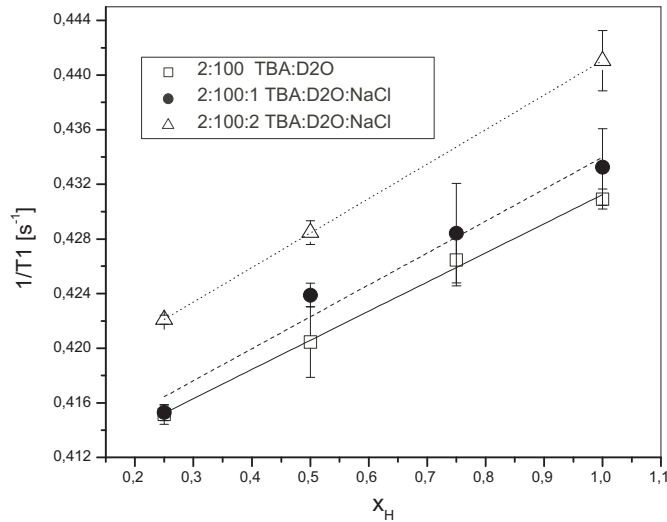


FIGURE 4.6: Relaxation rate  $1/T_1$  as a function of the isotopic dilution  $x_H$ . This plot is used to separate the intra- and intermolecular contributions to the relaxation rate. The intramolecular rate is the intercept with the  $y$ -axis and the intermolecular rate is the slope of the line.

The knowledge of the intermolecular relaxation time and the diffusion coefficient is not enough to evaluate the A-parameter. We need additionally

<sup>2</sup>The magnetic moment of the deuterium is smaller than that of the proton, this is characterized by the coefficient  $\alpha$

the number density  $\rho_H$ . This number can be calculated from the concentration [TBA] of TBA in Mol/m<sup>3</sup>. One molecule of TBA contains 9 protons, so the concentration of protons is 9 times that of TBA. Therefore, if  $\mathcal{N} = 6.022 \times 10^{23}$ /mol is the Avogadro's number, then the number of protons/unit volume is given by :

$$\rho_H = 9 \mathcal{N} [TBA]. \quad (4.35)$$

Here, the concentration of TBA can be determined via the relation,

$$[TBA] = \frac{\rho_{TBA} V_{TBA}}{V_{Total} M_{TBA}}, \quad (4.36)$$

where

$$V_{Total} = \frac{M_{Total}}{\rho_{Total}} \quad (4.37)$$

is the total volume of the solution. The associated density  $\rho_{Total}$ , is measured with the Anton Paar densimeter and,

$$M_{Total} = m_{NaCl} + \rho_{TBA} V_{TBA} + \rho_D V_D. \quad (4.38)$$

$V_{TBA}$ ,  $V_D$ ,  $\rho_{TBA}$  and  $\rho_D$  have the same meaning as in section 4.6.2 and  $m_{NaCl}$  is the mass of NaCl. The  $A$ -parameters obtained experimentally are given in Table 4.2.

## 4.7 Results and discussions

### Effect of NaCl

We performed nuclear magnetic relaxation experiments on aqueous solution of tertiary butanol with varying NaCl concentration while keeping the butanol concentration constant. Given a non-changing intermolecular dipolar relaxation time  $T_{inter}$ , an increasing relaxation rate would directly indicate an association behavior, whereas a decreasing relaxation rate would support the scenario obtained by Bowron and Finney. However, since the

correlation times are likely to be changing we follow the  $A$ -parameter approach proposed by Hertz and co-workers, discussed extensively in a separate section above. The  $A$ -parameter approach is based on the assumption of a linear relationship between the intermolecular dipolar relaxation time  $T_{\text{inter}}$  and the inverse self-diffusion coefficient of the solute molecules, which can be obtained independently. The diffusion coefficients were measured by the PGSE technique [32,34]. The gradient calibration was done as described in section 2.6.2. In addition, the experimental self-diffusion coefficients for TBA-d1 in heavy water/salt solutions are shown in Table 4.2. The diffusion coefficient decreases as the salt concentration increases. From the diffusion result we might anticipate the effect, induced by NaCl. Since small aggregates might diffuse faster than large ones, it appears that TBA-TBA intermolecular forces are modified such that TBA clusters are formed.

Hence we extracted the inter- and intramolecular dipole-dipole relaxation rate for the aliphatic hydrogens by the isotopic dilution technique. A qualitative description of the intra-/ intermolecular contributions and the observed relaxation times  $T_1$  are given in section 4.4.1.

TBA-d1:D <sub>2</sub> O:NaCl	2:100:0	2:100:1	2:100:2
$\rho/\text{kg m}^{-3}$	1083.9	1106.1	1122.5
$c(\text{TBA})/\text{mol l}^{-1}$	1.0059	0.9994	0.9882
$c(\text{NaCl})/\text{mol l}^{-1}$	-	0.5270	1.0403
$T_{1,\text{inter}}/\text{s}$	$44.89 \pm 1.74$	$41.02 \pm 4.73$	$37.92 \pm 0.13$
$D/10^{-9}\text{m}^2\text{s}^{-1}$	0.3962	0.3818	0.3709
$A/10^{-39}\text{m}^5\text{s}^{-2}$	1.619	1.718	1.826

TABLE 4.2: Experimental densities  $\rho$ , intermolecular relaxation times  $T_{1,\text{inter}}$  and self-diffusion coefficients  $D$  for TBA-d1 in TBA-d10/D<sub>2</sub>O/NaCl solutions. All experiments were carried out at  $T = 25^\circ\text{C}$ . Also given are the TBA-d1 concentrations and the obtained  $A$ -parameters.

Fig. 4.7 shows the plot for the  $A$ -parameter. We observe an increase of the  $A$ -parameter upon addition of NaCl. Moreover, an apparent linear relationship is observed within the salt concentration range. Measurement at



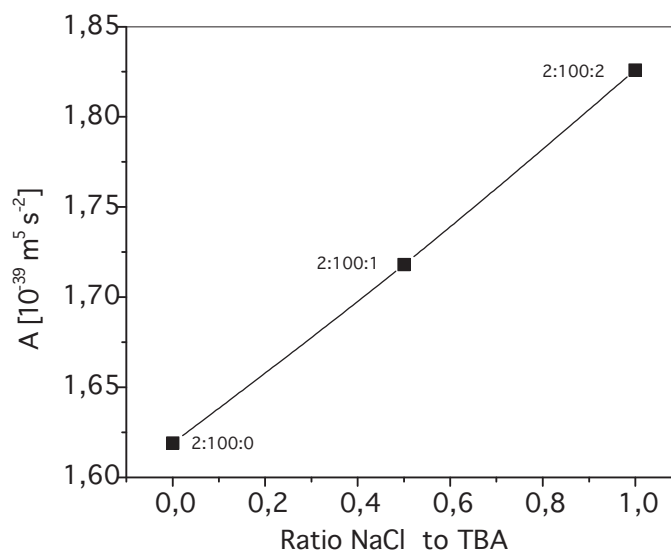


FIGURE 4.7: Evolution of the A-parameter vs the NaCl concentration.

high salt concentration might give more information on this dependence.

The molecular dynamics results indicate a significant increase of the height of the peak of the central carbon pair correlation function upon adding NaCl, see Fig. 4.8. It follows an increase of the number of nearest neighbors of the TBA molecule which means an increase of the degree of association, that is an enhancement of the hydrophobic contact of the TBA molecule with increasing salt concentration. More details on the MD can be found in ref. [83]. Both A-parameter and MD results indicate that the NaCl enhances the self-association tendency of the TBA molecules. However the result of Bowron and Finney [12,70] using the neutron scattering technique predict a significant decrease of the height of the the peak upon adding salt. This decrease, accompanied by an increase at a distance of a second neighbor peak located at about 0.85nm, lead to the conclusion that the anion ( $\text{Cl}^-$ ) bridge TBA pair. On the other hand, there is no evidence for such bridging from the MD point of view. Unfortunately we do not have any NMR experiment at hand that can allow us to support this result.

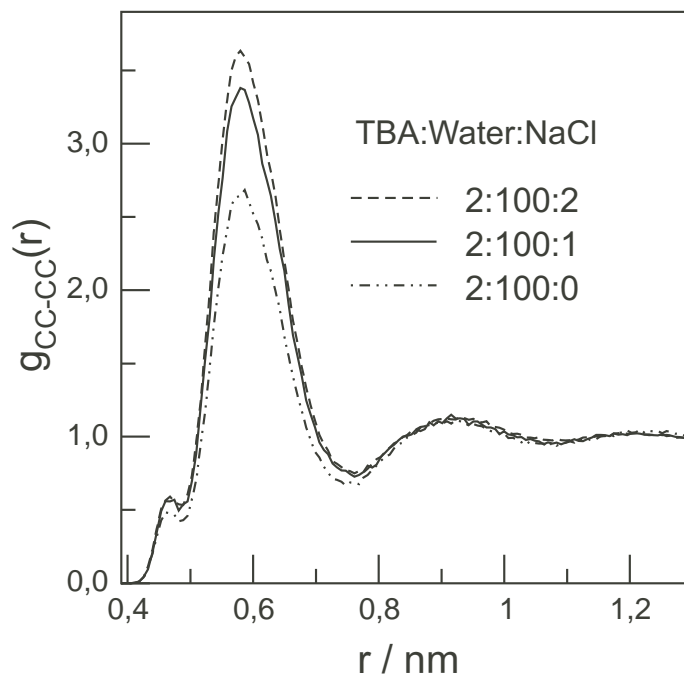


FIGURE 4.8: Radial pair distribution functions between the TBA central carbon atoms (CC) in aqueous solutions at different salt concentrations, from MD simulation [83].

	$x_H$	1.0	0.75	0.5	0.25
TBA:D2O:NaCl					
	2:100:0	2.321	2.345	2.378	2.409
	2:100:2	2.267	-	2.334	2.369
	2:100:4	2.230	2.321	2.348	2.373
TBA:D2O:NaBr					
	2:100:2	2.306	2.325	2.351	2.375
	2:100:04	2.283	2.310	2.335	2.366
TBA:D2O:NaI					
	2:100:2	2.348	2.377	2.391	2.415
	2:100:4	2.405	2.425	2.445	-

TABLE 4.3: Some dilution data. The number represent the relaxation times in seconds.  $x_H$  is the dilution parameter defined by Eq. (4.24)

Samples	$T_1$	$T_{1,intra}$	$T_{1,inter}$	$D/10^{-10}\text{m}^2\text{s}^{-1}$	$A/10^{-39}\text{m}^5\text{s}^{-2}$
TBA:D <sub>2</sub> O:NaCl					
2:100:0	2.321	2.445	44.889	3.962	1.628
2:100:2	2.267	2.411	37.920	3.709	1.853
2:100:4	2.230	2.447	27.853	3.546	2.475
TBA:D <sub>2</sub> O:NaBr					
2:100:2	2.306	2.403	56.002	3.882	1.319
2:100:4	2.283	2.398	47.506	3.798	1.569
TBA:D <sub>2</sub> O:NaI					
2:100:2	2.348	2.441	63.727	4.157	1.254
2:100:4	2.405	2.491	69.646	4.196	1.202

TABLE 4.4: Summary of the experimental quantities including the calculated  $A$ -parameters. The sample 2:100:0 is the reference and therefore is salt free. The relaxation times are in seconds. All experiments were carried out at  $T = 25^\circ \text{C}$ .

### Effect of NaBr and NaI

In this section, the component in the mixture (TBA:D<sub>2</sub>O:Salt) are in the ratio: 2:100:0, 2:100:2 and 2:100:4. We decided to increase the salt concentration to really appreciate the effect that salts can induce. We made also samples with high NaCl concentration to be used as reference regarding the discussion. The dilution data are given in Table 4.3. The relaxation times increase as the proton concentration is diluted. This observation fits our expectation, i.e a decrease of the number of dipoles leads to an increase of the relaxation time.

The diffusion results presented in Table 4.4 are discussed at the first place. As shown in Fig. 4.9, diffusion coefficients have different behaviors. For TBA:D<sub>2</sub>O:NaCl, we observed that the more we increase the NaCl concentration, the diffusion coefficient decreases. So the discussion above might still hold, at least for the range of concentrations that we have investigated. Now if we consider the sample TBA:D<sub>2</sub>O:NaBr, we see also a similar evolution of the diffusion coefficient, although at a moderate rate. Thus, we might be able to draw a conclusion very close to that of TBA:D<sub>2</sub>O:NaCl. However, TBA:D<sub>2</sub>O:NaI presents a totally different behavior. In fact the dif-

fusion coefficient of TBA increases with the increase of the concentration of NaI. That is, NaI might break the existing structure of TBA, and by this fact enhance the mobility of the molecule. Every time the behavior of NaBr is in-

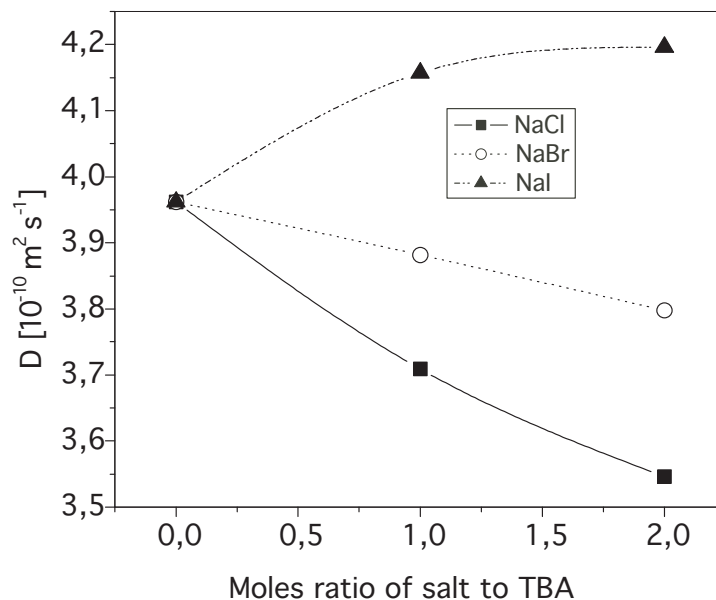


FIGURE 4.9: Dependence of the diffusion coefficient as a function of salt concentration.

termediate between that of NaCl and that of NaI. But the induced deviation is more pronounced in the NaCl direction.

To determine the A-parameter for these data, we needed also to measure the density of the sample. We did not use the densimeter, rather we estimated the number density  $\rho_H$  via Eq. (4.35) and (4.36), except that in the last equation the approximation is  $V_{Total} \approx V_{TBA} + V_{D2O} + V_s$  (the incompressibility of the fluid mixture justifies the approximation), with  $V_s = m_s/\rho_s$ . Using these relations, we were able to evaluate the A-parameter for each sample. The quantitative results are found in Table 4.4. The first two rows were already determined previously (see Table 4.2), but here we reported only the calculated values to homogenize the results. Fig. 4.10 is an illustration of the evolution of the A-parameter as a function of different salts. The result for the A-parameter confirms the discussion for the diffusion coefficient, that is NaCl and NaBr might enhance the initial structure of TBA molecule by

enhancing the hydrophobic contact while NaI plays the opposite role.

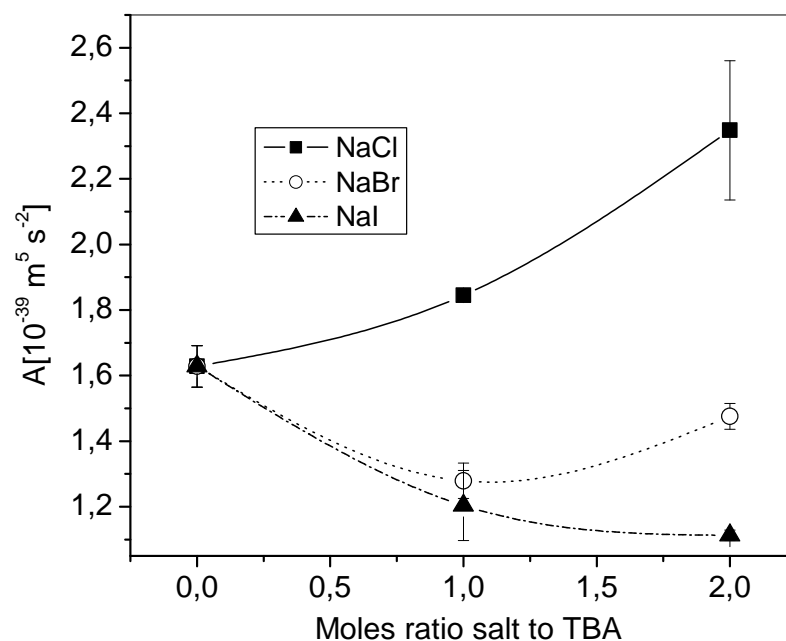


FIGURE 4.10: Evolution of the A-parameter. The curve are splines

## 4.8 Conclusions

We have used nuclear magnetic resonance A-parameter measurements to investigate the effect of salt (NaCl, NaBr and NaI) on the association-behavior of tertiary butanol molecules in an aqueous solution. Molecular dynamics simulations have been used to calibrate the result for the sample containing NaCl, moreover a detailed structural characterization of the MD-simulation data [83] does not hence provide evidence for a significant amount of chloride-bridged butanol-pairs, as recently proposed from the analysis of neutron experiments [12, 70]. We have shown that an increasing NaCl and NaBr concentration is found to further strengthen the solute-solute hydrophobic interaction, whereas an increasing NaI concentration lowered the TBA-TBA interaction. Finally we would like to emphasize that the mechanistic picture

introduced by Bowron and Finney still remains an interesting and challenging concept, and might be applicable in case of relatively larger anions such as iodide.

---

# Effect of Salts on Model Biomembranes

---

### 5.1 Introduction

Membranes are the most common cellular structures in both animal and plants Fig. 5.1. Their function is vital for living cells because they are involved in almost all aspects of cellular activity, ranging from compartmentalization to selective passage of metabolites in and out of the cell. For example, the plasma membrane is the envelope of the cell and controls the movement of substances into and out of a cell. The endoplasmic reticulum forms a network of folded membranes within the cytoplasm. Mitochondrial and chloroplast membranes convert organic materials into energy in the cell. The nuclear membrane separates the genetic substance (DNA in particular) from the cytoplasm in the cells [88]. It appears that most membranes are structured bilayers of amphiphilic molecules and are built up

according to the general principles of liquid crystal structures [9,89].

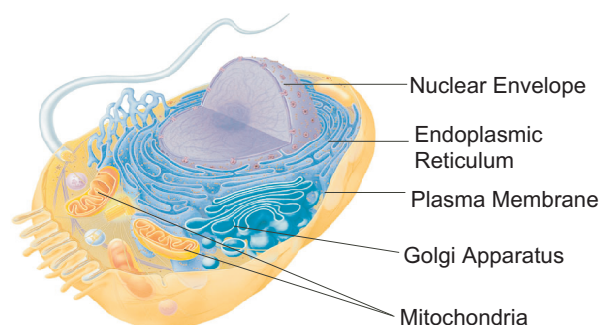


FIGURE 5.1: Illustration of an animal cell. All components are separated by membranes

Biological membranes are formed as a result of hydrophobic interactions of lipid molecules in solution. Most of the time, the solution contains salt with different concentrations. Salts influence several properties of aqueous solutions, specially the self-association behavior or hydrophobic contacts. The cation plays a significant role in the interaction of salt with lipids [14], as opposed to the alcohol molecule where the association behavior is believed to be driven by the anions [12,70]. In order to understand the effect of salt, it is important to monitor not only the effect the salt can induce in the system, but to identify where the salt is residing (located) in the system.

We used NMR to study the relatively simple model system of biomembrane  $C_{12}E_5$  as a function of the concentration of NaCl, NaI and temperature.

## 5.2 Model Biomembranes

The natural cell membrane is an extremely complex structure in which various functional entities (channels, receptors) are embedded. The degree of complexity has induced researchers to resort to simpler model systems in order to comprehend and to explain the structure and function of natural membranes [9,90].



The cell membrane model is a two dimensional liquid crystalline lipid bilayer, formed in water as a result of self-assembling process occurring as described in paragraph 3.4, that is the hydrocarbons form an oily core whereas the polar groups remain at the surface in contact with water.

It is worth recalling that liquid crystals or mesophase [91], are substances that exhibit phase properties in between the crystalline solid and simple liquid, that is a liquid crystal may flow like a liquid, but have the molecules in the liquid arranged and oriented in a crystal like way. The basic characteristic of liquid crystals is the presence of orientational order of the anisotropic molecules, and the limited positional order. The orientational order is the ability of molecules to point their axes in specific direction known as director while the positional order is the ability of molecules to occupy specific sites in a lattice. The quantity of order is measured by an order parameter.

Liquid crystals exhibit a polymorphic character. Thus, the phase transition may be induced either as a function of the temperature and they are called thermotropics, or as a function of the concentration and they are called lyotropics. Many basic biomolecules (lipids, proteins, nucleic acids) possess a lyotropic liquid crystalline phase, either pure or mixed. Here, our investigation is limited to lyotropic liquid crystals.

### 5.2.1 Lyotropic liquid crystalline phases

Lyotropic liquid crystals are formed by dissolution of amphiphilic molecules of a material in water <sup>1</sup>, i.e they consist of two or more components. The molecular structures of amphiles or lipids (two distinct parts with different properties in the same molecule inducing an anisotropic character required for liquid crystal formation) confers them the ability to form lyotropic crystalline phases. As the concentration of the amphiphile material increases, intermicellar interactions become significant and the micelles rearrange to form ordered structures. There exist several different types of lyotropic liq-

---

<sup>1</sup>Note that thermotropics are single component substances.

liquid crystal phase structures determined by the concentration of the solute compound in the solvent [54,88,91].

Possible phase structures are the hexagonal phase, Fig. 5.2, consisting of rod-shaped micelles, packed in a hexagonal array and separated by continuous water region. Two hexagonal phase structures are known: the normal hexagonal phase and the reverse hexagonal phase having the hydrocarbon chain occupying the spaces between the hexagonally packed water cylinder. The spacing between cylinders depend on the water contents.

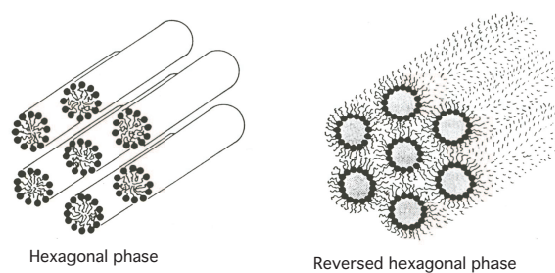


FIGURE 5.2: Hexagonal lyotropic liquid crystalline phases. The amphiphiles form long cylinders arranged into an hexagonal lattice.

The cubic phase (or viscous isotropic phase) structure is not well established and appears mainly in the phase transition zones between the hexagonal and lamellar phases. The known cubic phase exhibits a cubic arrangement of molecular aggregates as shown on Fig. 5.3

The third and most important structure in biology is the lipid bilayer.

### 5.2.2 Lipids and Bilayer Structure

Lipid molecules are a particular kind of amphiphile. In addition to their anisotropic character ( e.g. rod like shape), they possess high enough mass. These properties confer lipids the ability to form liquid crystalline phase.

The formation of lipid bilayers is a rapid and spontaneous process, with the hydrophobic interactions as the main driving force. Water molecules are released from the hydrophobic tails as these tails become sequestered in the interior of the bilayer. Additionally, the van der Waals attractive forces

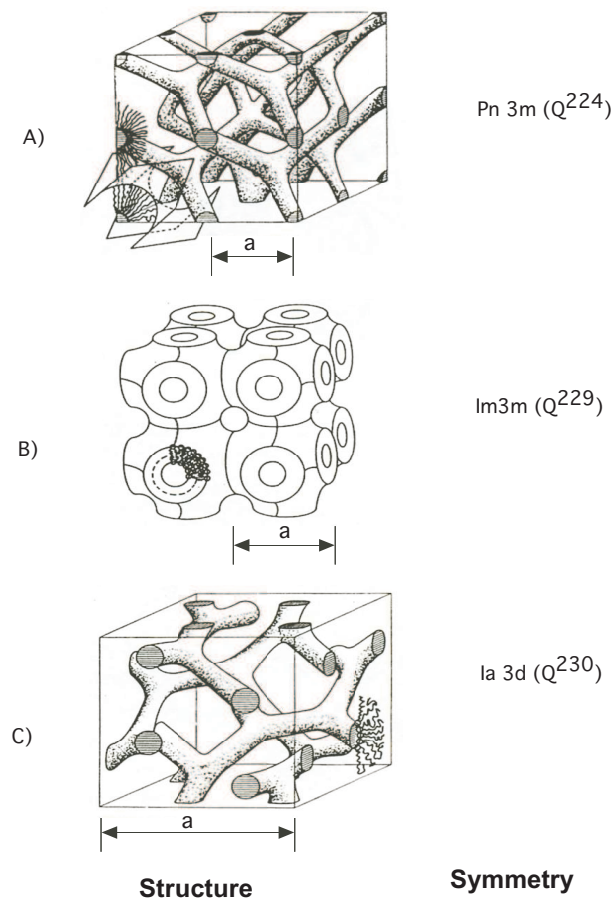


FIGURE 5.3: Well-established inverse bicontinuous cubic phases indicating different space group symmetry,  $a$  is the lattice parameter. A) The double diamond phase. B) The plumber's nightmare cubic phase. C) The gyroid cubic phase. Adapted from Petrov, [88]

between the tails favor a close packing. And finally, the lipid bilayers are stabilized by the electrostatic interactions and the formation of hydrogen bonds in the head group region. The lamellar phase, also known as neat

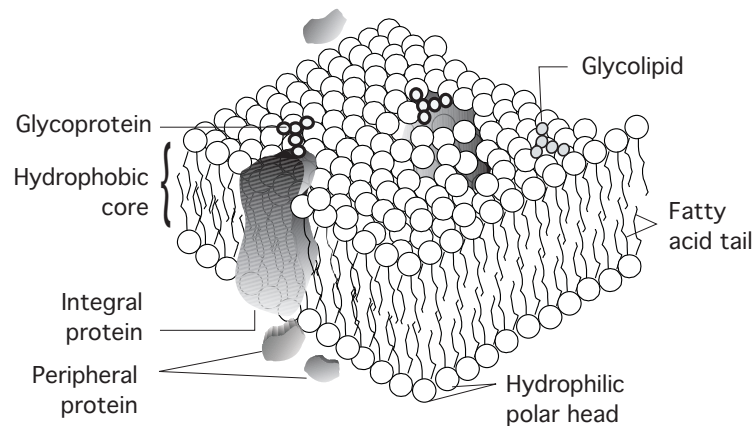


FIGURE 5.4: Fluid mosaic model of biomembranes. The matrix of the membrane is formed by phospholipids. Some integral proteins contain hydrophilic groups on both ends and traverse the membrane thickness. The peripheral membrane are mainly hydrophilic and interact with the membrane faces by electrostatic interaction.

phase, presents the amphiphilic molecules arranged in bilayers separated by water layers. The bilayer thickness is larger than a molecular length and their monolayers are not interdigitated.

The common representation of biological membranes is the bilayer structure of Singer and Nicolson [9], suggesting that the membrane is not a static two-dimensional crystal, but it is a highly dynamic system with many types of motion. This model is known as "fluid mosaic", indicating that the molecules within the membrane have considerable lateral and rotational freedom and therefore are randomly distributed within the membrane. The fluid mosaic model essentially consists of large phospholipid with embedded protein, Fig. 5.4. The phospholipids are arranged to form bilayers of lipid amphiphiles molecules with their hydrophilic part in contact with the aqueous phase while the hydrophobic carbon chains of both monolayers meet at the center of the bilayer and are shielded from water. The proportion of protein and lipid can vary widely according to the type of membrane,

but the common constituents of all membranes are lipids with long hydrocarbon chains.

The hydrophilic head groups vary considerably between different membranes, but the hydrocarbon tails are long and contain both saturated and unsaturated hydrocarbons.

Membrane lipids are fluid and offer little resistance to bending while membrane proteins are rigid and affect lipids in their vicinity when incorporated into a lipid bilayer.

### 5.2.3 Magnetic Field Induced Orientation

Sample orientation is a routine practice in solid state NMR. By this means, the resolution of spectra can be improved significantly, for instance powder patterns are avoided while retaining the structural parameters observed in solids. The orientational techniques include sample spinning (MAS) about the magic angle of  $54.7^\circ$ ; the mechanical orientation consisting of sandwiching the sample between juxtaposed glass surfaces. Besides these techniques, orientation may be also induced by the use of an anisotropic media (liquid crystal).

Biomolecules such as lipids and proteins orient spontaneously in a magnetic field. The origin of orientation is believed to be the anisotropy of the diamagnetic susceptibility tensor,  $\chi$  [92, 93]. When model membrane systems are prepared in the form of lipid bilayer and placed in a magnetic field, the field  $B_0$  induces on the molecules a magnetic moment proportional to  $\chi$ . The susceptibility  $\chi$  is negative and small for ions and diamagnetic molecules, but positive and larger for paramagnetic species. The anisotropy of bilayer constituents infers a tensor character to the magnetic susceptibility.

The degree of orientation of rotational symmetry axis  $i$  in the molecule relative to  $B_0$  is measured by the parameter  $S_{iB}$  defined by [93]:

$$S_{iB} = \left\langle \frac{3 \cos^2 \theta_{iB} - 1}{2} \right\rangle \quad (5.1)$$

where  $\theta_{iB}$  is the angle between the axis  $i$  and  $B_0$ . An expression for  $S_{iB}$  can be derived under the assumption that the change in energy of the system upon putting a molecule in the magnetic field obey Boltzmann distribution [93]. Then,

$$S_{iB} = \frac{\Delta\chi_{ii}B_0^2}{15\mu_0k_B T} \quad (5.2)$$

where  $\Delta\chi_{ii} = \chi_{ii} - (\chi_{jj} + \chi_{kk})/2$  is the difference between the susceptibilities parallel and perpendicular to the axis of rotational symmetry,  $k_B$  is the Boltzmann constant,  $T$  the absolute temperature. The degree of orientation is proportional to the square of the static magnetic field  $B_0$  and is inversely proportional to the temperature.

Eq. (5.1) and (5.2) are defined on individual molecules. However, the macroscopic alignment results from the interaction of the applied field with the collective diamagnetic susceptibility of the isolated bilayer domain. So the degree of alignment of the bilayer is given by :  $S_{iN} = N_i S_{iB}$  where  $N_i$  is the number of the nuclei in the domain. The order parameter can be directly related to certain experimental quantities [26, 88]. For example, in deuterium NMR, the quadrupole splitting is related to the order parameter  $S_{iN}$  by

$$\Delta\nu_Q = \frac{3}{2} \frac{e^2 q Q}{h} S_{iN}. \quad (5.3)$$

where the constants are the same as in Eq. ( 2.14).

In the liquid crystalline phase which characterizes many membrane preparations, macroscopic alignment may or may not occur depending on the competition between the magnetic torque, the thermal motion and viscous force [94]. The magnetic contribution tends to make the local order director of the liquid crystal align either parallel (for samples with  $\Delta\chi > 0$ ) or perpendicular (for samples with  $\Delta\chi < 0$ ) to the magnetic field. The other contribution tends to counteract this alignment, particularly these effects prevail at high surfactant concentration (e.g.  $L_\alpha$  phase) making magnetic alignment not so easy. Traditionally, the alignment is induced by a thermal cycle that is heating the sample above their anisotropic phase transition and

leaving them cool down gradually, of course in the presence of the magnetic field. The heating serves to reduce the effect of the viscous and elastic forces.

The dipolar and quadrupolar interactions are mainly responsible for the modification of the NMR spectrum upon alignment of the molecule. Both vanish in an isotropic medium.

#### 5.2.4 Material: the pentaethylene glycol monododecyl ether

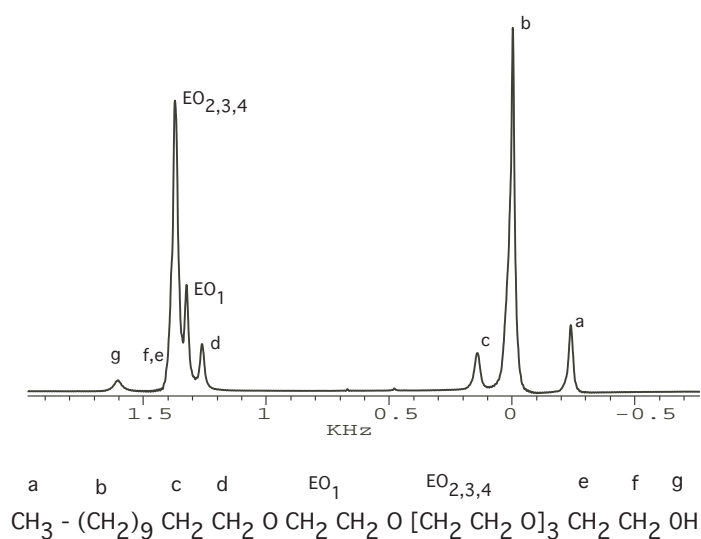


FIGURE 5.5: Proton spectrum of pure  $\text{C}_{12}\text{E}_5$  at  $25^\circ\text{C}$  recorded on a 600MHz spectrometer, the peaks assignment and the nomenclature used in the text to refer to specific protons. The peak assignment is adapted from ref. [95]

The pentaethylene glycol monododecyl ether molecule ( or  $\text{C}_{22}\text{H}_{46}\text{O}_6$ , and its short name is  $\text{C}_{12}\text{E}_5$ ) shown in Fig. 3.5, is a non-ionic amphiphilic molecule. The NMR spectrum of  $\text{C}_{12}\text{E}_5$  is shown in Fig. 5.5 together with an assignment of the various signals, adapted from a previous work on the same sample, on a 360 MHz spectrometer [95]. The alkyl chain plays the role of the hydrophobic region or tail, whereas the oxyethylene group ( $\text{EO}_1$ ,  $\text{EO}_{2,3,4}$ ) is the hydrophilic region.

The various phases of  $\text{C}_{12}\text{E}_5$  solution can transform from one to another by changing the solution conditions such as the solute (solvent) concentration or the temperature. Usually a phase diagram is associated to the struc-

tural changes brought about, see Fig. 5.6. The focus of the present study is on the lamellar phases.

The lamellar phase ( $L_\alpha$ ) exist over a broad temperature and concentration range (cf. Fig. 5.6). One can distinguish a highly dilute amphiphile phase (down to 1% wt  $C_{12}E_5$ ) and a concentrated amphiphile phase ( $\gtrsim 60\%$  wt  $C_{12}E_5$ ), both being interconnected continuously [96,97].

The phase diagram of Fig. 5.6 was established using  $H_2O$  as solvent. The investigation of the molecular and phase structure of the system  $C_{12}E_5$  indicate that the lamellar phase is stabilized by the presence of interlamellar water [98]. But we do not use  $H_2O$ , instead we replace  $H_2O$  by  $D_2O$ . It is known that this replacement results in a lowering of the various transition temperatures [96]. More importantly, the formation of the dilute  $L_\alpha$  phase is favored in the presence of  $D_2O$ , whereas, the phase behavior at high surfactant concentration is not influenced by the substitution of  $H_2O$  by  $D_2O$  [97].

### 5.2.5 Sample Preparation

The pentaethylene glycol monododecyl ether was purchased from Sigma-Aldrich Chemie GmbH. The solvent  $D_2O$  with the purity 99.96% was obtained from Merck KGaA Germany. The solution was prepared in the  $L_\alpha$  phase according to the phase diagram of Fig. 5.6, by weighing the different components ( $C_{12}E_5$ ,  $D_2O$  and salts). The mass of  $C_{12}E_5$  ( $m_P$ ) and the mass of  $D_2O$  ( $m_D$ ) obey the relation

$$x_P \cdot m_D = x_D \cdot m_P, \quad (5.4)$$

where  $x_P$ ,  $x_D$  are the mass fraction of  $C_{12}E_5$  and  $D_2O$  respectively. We can write also  $m_D = \rho_D \cdot V_D$ , where  $\rho_D = 1.107\text{g/ml}$  is the density of  $D_2O$ . It follows the volume of  $D_2O$  to be measured for a given mass  $m_P$  of  $C_{12}E_5$  is given by :

$$V_D = \frac{(1 - x_P)}{x_P} \cdot \frac{1}{\rho_D} \cdot m_P, \quad (5.5)$$

since  $x_P + x_D = 1$  in the solution.



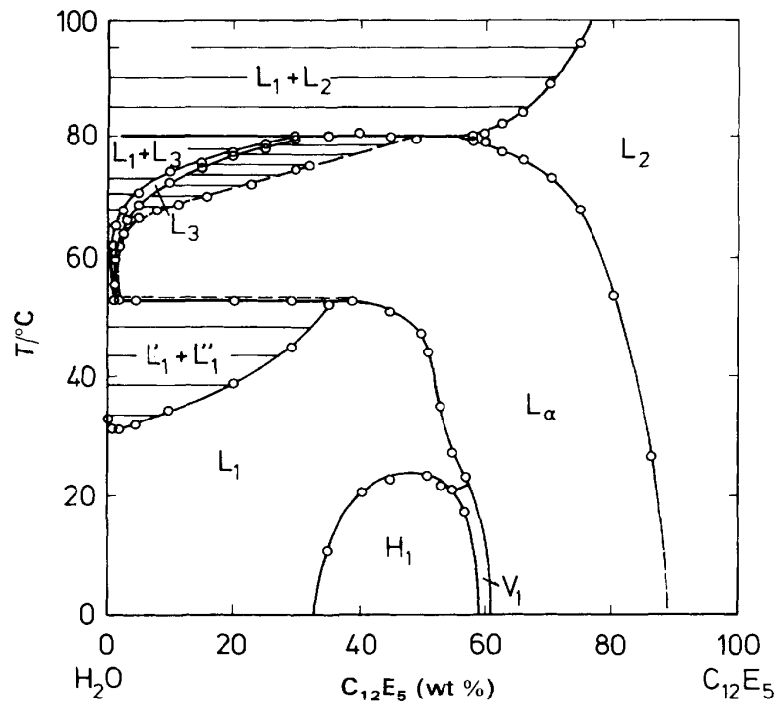


FIGURE 5.6: Phase diagram of the  $C_{12}E_5$ -water system over the temperature range  $0 - 100^\circ\text{C}$ .  $L_1$ ,  $L_2$  and  $L_3$  denote isotropic liquid solutions,  $H_1$  is a normal hexagonal phase,  $V_1$  is a cubic liquid crystalline phase and  $L_\alpha$  denotes a lamellar liquid crystalline phase [96]

Sample No	$x_P$	$x_s$	$m_P$ (g)	$V_D$ ( $\mu\text{L}$ )	$m_{NaCl}$ (g)	$m_{NaI}$ (g)
S1	0.5	0.0	0.2452	221.500	-	-
S2	0.5	1.0	0.2562	231.436	0.03682	-
S3	0.5	1.0	0.2486	224.571	-	0.09165
S4	0.7	0.0	0.3494	135.269	-	-
S5	0.7	0.5	0.3041	117.731	0.02185	-
S6	0.7	1.0	0.4346	168.254	-	0.16022
S7	0.8	0.0	0.4473	101.016	-	-
S8	0.8	0.5	0.4973	94.196	0.0299	-
S9	0.8	1.0	0.4100	92.526	-	0.15113

TABLE 5.1: Sample composition. Because of the low solubility of NaCl (35.9g/100ml, with respect to water),  $x_s = 0.5$  to have an homogeneously mixed solution. The solubility of NaI is rather high (184g/100ml) and the ratio  $x_s = 1$  is maintained for all samples containing NaI.

The quantity of salt is determined by the relation

$$m_s = x_s m_P \frac{M_s}{M_P} \quad (5.6)$$

where  $x_s$  is the ratio of the number of moles of salt to the number of moles  $\text{C}_{12}\text{E}_5$ ,  $m_s$  is the mass of salt,  $M_s$  and  $M_P$  is the molar mass of salt and  $\text{C}_{12}\text{E}_5$  respectively. The sample composition is given in Table 5.1.

The homogenization processes was made by heating the mixture in a water bath at 45-75°C for a long time ( more than ten minutes), then shaking vigorously. The process was repeated several times. The sample was frozen in liquid nitrogen, and flame sealed. NaI turns the color of  $\text{C}_{12}\text{E}_5$  solution from transparent to slightly colored in gold.

### 5.3 Deuterium Magnetic Resonance ( $^2\text{H}$ NMR)

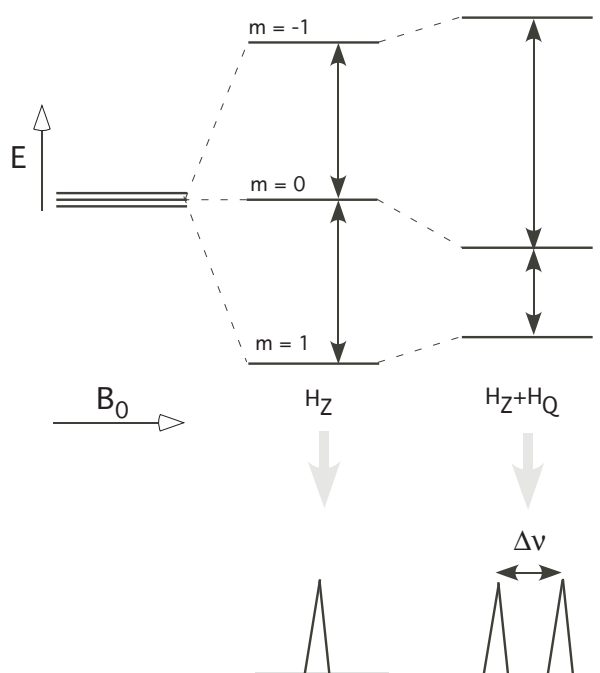


FIGURE 5.7: Energy levels of a deuterium nuclear spin ( $I = 1$ ) with and without the influence of the quadrupole coupling. The allowed transitions and corresponding splittings are shown.

In many situations, the spectrum of the lipid is dominated by strong

proton-proton and proton-carbon dipolar interactions. As a result the spectra contain a large number of overlapping resonances and are rather difficult to analyze. The structure and dynamics of molecular system can be monitored alternatively by deuterium NMR [26,90].

Deuterium has nuclear spin  $I = 1$  and therefore possesses a quadrupole moment that defines the non spherical distribution of nuclear charges. The Hamiltonian  $H$  for the deuterium nucleus in a magnetic field is given by

$$H = H_0 + H_Q, \quad (5.7)$$

where  $H_0$  is the zeeman Hamiltonian and  $H_Q$  is the quadrupole Hamiltonian defined by Eq.(2.13) is orientation dependent. The quadrupole interaction is a weak perturbation of the Zeeman interaction so that the corresponding energy levels can be easily estimated by perturbation theory. These energy levels are shown in Fig. 5.7.

Traditionally, some hydrocarbon atoms in the lipid chain are replaced by deuterium, and it follows that the spectra of partially deuterated molecules consist of a few resonances with respect to the corresponding proton spectra. However to gain the full possibility of deuterium NMR, one should be able to synthesize accurately the molecules deuterated at the desired positions. But this task is not always straightforward. More often people used the commercially available products. This makes some restrictions in the range of lipid membranes to be investigated.

The basic features of deuterium NMR exploited for our investigation reside in the fact that  $^2\text{H}$  NMR can easily detect anisotropic motions in the system. For a rapid isotropic motion, the deuterium NMR spectrum consist of one single line, while for an anisotropic motion each deuteron contributes a doublet due to the quadrupole moment of the deuterium nucleus. The doublet spacing  $\Delta\nu_Q$  defined by Eq. (2.14), depends on the degree of anisotropy and the reorientation of the deuteron with respect to the molecular symmetry axis. In oriented samples, the quadrupole splitting depends further on the angle between the magnetic field and the axis of motional averaging (director axis), Fig. 5.8.

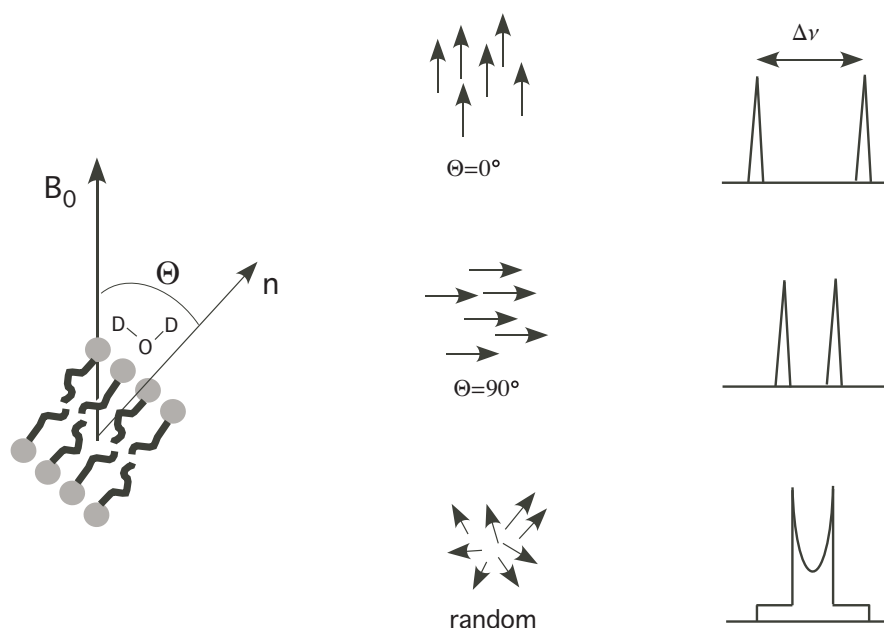


FIGURE 5.8: Orientation of a bilayer in the magnetic field and the possible lineshapes.  $n$  is the director of the bilayer. The bound water sit on the head groups.

Actually, the pentaethylene glycol monododecyl ether deuterated at the desired position is not readily available to purchase. So, the  $^2\text{H}$  of  $\text{D}_2\text{O}$  is measured during the experiment. In fact,  $\text{D}_2\text{O}$  can participate in the anisotropic motion of the solute molecule [97, 99]. There exists two types of water molecules: the free water that is free to move and the bound water that is in contact with the polar group of the surfactant molecule. Because of the fast exchange between both types of water, only an average motion is detected. Therefore, a splitting is an indication that the average motion of the  $\text{D}_2\text{O}$  molecules is anisotropic. It is then possible to determine region of phase coexistence of the lamellar phase with an isotropic phase. The splitting of the  $^2\text{H}$  NMR signal is a measure of the degree of order in the  $L_\alpha$ , which helps in discussing the structural change.

## 5.4 Experimental Considerations

The sample temperature was maintained by the spectrometer temperature controller which has been calibrated by direct insertion of a thermocouple into the sample location inside the probe-head (see Fig. 4.5). A thermal cycle was used to improve the alignment of the liquid crystalline phases. During the heating process,  $^2\text{H}$  NMR measurements were carried out to measure the degree of orientational ordering. At each temperature, the samples were allowed to equilibrate for at least 15 min.

Deuterium NMR measurements were performed using a Varian 600 MHz spectrometer. All data were obtained using a single pulse sequence  $90 -$  acquisition with pulse length of  $26 - 30\mu\text{s}$ . The FID following a single  $90^\circ$  excitation pulse was long enough and largely detectable to make the use of quadrupolar echo pulse sequence ( $90_x - \tau - 90_y$ ) unnecessary. The relaxation times were in the order of  $0.5 - 0.7\text{s}$ . The dead time was set to  $5\mu\text{s}$ . A recycle delay of 2s and 5 – 50 accumulations were necessary to obtain good signals.

## 5.5 Results and Discussions

### Lineshape Analysis

Fig. 5.6 shows the phase diagram of the surfactant used in our investigation. A systematic study of the effect of salt on the phase diagram of chromonic liquid crystals have been done earlier [100].

We start studying the samples with low surfactant content (50% wt  $\text{C}_{12}\text{E}_5$ ). For this concentration and from the phase diagram we know that the lamellar phase occurs at temperature  $\geq 50^\circ\text{C}$ . So we start the heating process from the ambient temperature ( $25^\circ\text{C}$ ) to  $50^\circ\text{C}$ , where the lamellar phase is supposed to start to form. The change in the spectra brought about by the salt at some temperatures is shown in Fig. 5.9. We were then able to observe simultaneously the changes induced by temperatures and salts.

The temperature of  $25^\circ\text{C}$  is very close to the boundary hexagonal-isotropic

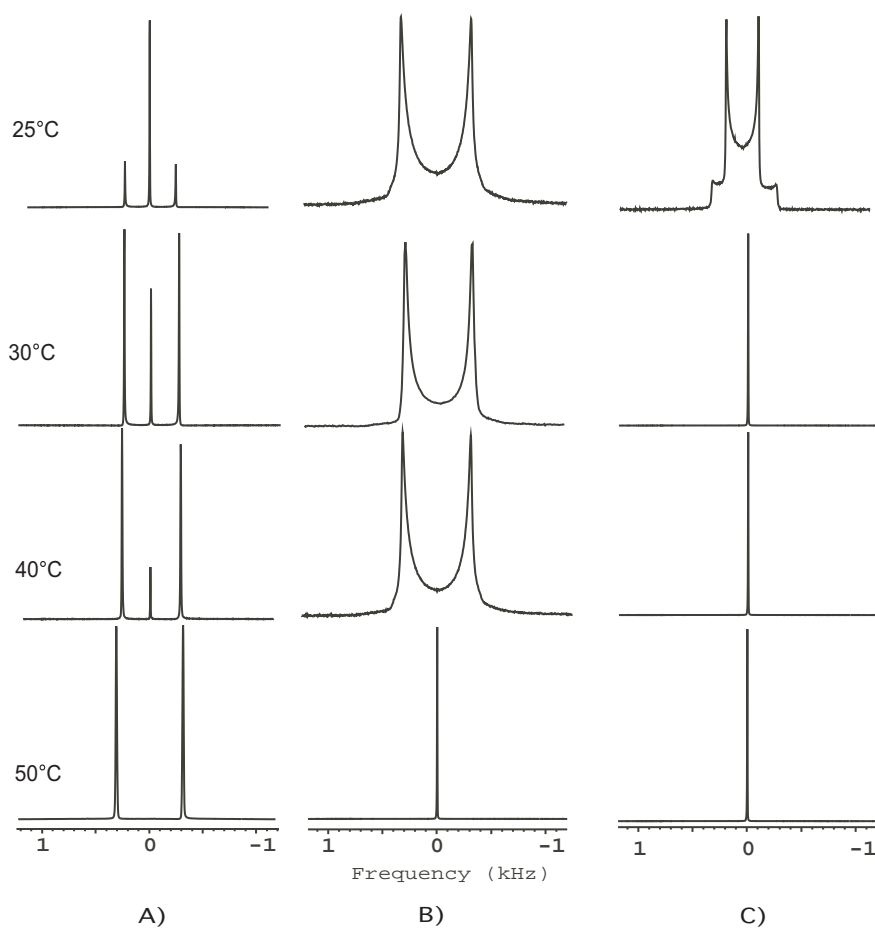


FIGURE 5.9: Deuterium spectra of 50 wt %  $C_{12}E_5$  as a function of the temperature. A)  $C_{12}E_5:D_2O$ . B)  $C_{12}E_5:D_2O:NaCl$ . C)  $C_{12}E_5:D_2O:NaI$

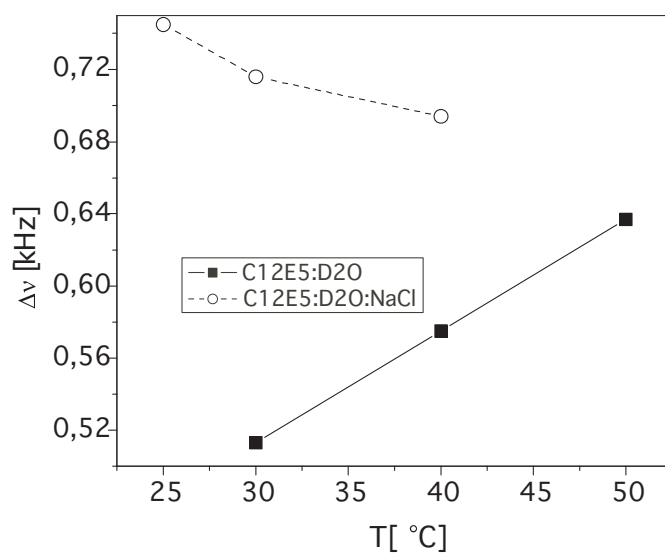


FIGURE 5.10: Variation of the quadrupolar splitting

$L_2$  phase. This might explain the presence of the residual splitting observed on Fig. 5.9 A) at 25°C. Upon heating, there appears more and more anisotropic domain. At 50°C, the isotropic phase is almost gone and the anisotropic lamellar phase prevails as predicted by the phase diagram.

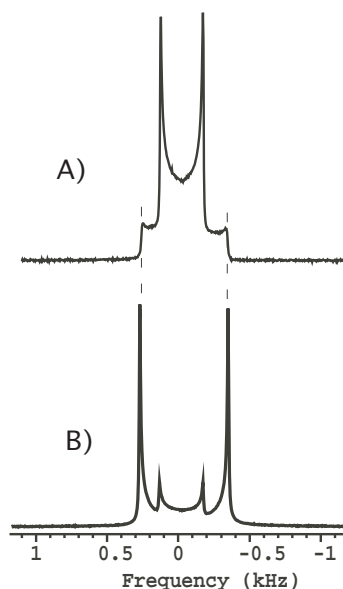


FIGURE 5.11: The spectral shape transformation in the magnetic field (50 wt %  $C_{12}E_5$ ). All the spectra were measured at 25°C: A) Before heating to the isotropic phase. B) After cooling from the isotropic phase

When NaCl is added, it induces a splitting already at 25°C, Fig. 5.9 B), and the splitting remains over a wide temperature range. The baseline of these spectra is very broad. The splitting is larger than that of the reference sample (sample without salt) and decreases when the temperature increases, Fig. 5.10. The phase boundary is shifted upward by more than 25°C. The isotropic phase occurs only at temperatures higher than 40°C.

The effect of NaI is quite different from that of NaCl as expected from the measurement on TBA (see chap. 4). At 25°C, a powder-like spectrum is obtained. However, this spectrum does not survive a temperature increase of 5°C, Fig. 5.9 C). At 30°C, the sample shows an isotropic structure, and the temperature of the upper isotropic-lamellar phase boundary is shifted upward. After cooling the sample from the isotropic phase to the initial

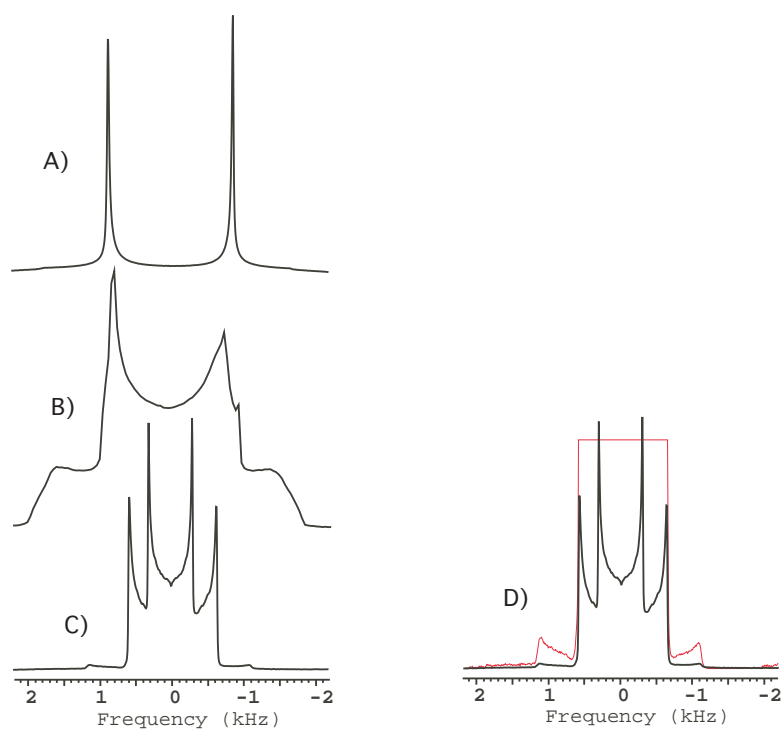


FIGURE 5.12: Deuterium spectra of 70 wt %  $C_{12}E_5$ . A)  $C_{12}E_5:D_2O$ . B)  $C_{12}E_5:D_2O:NaCl$ . C)  $C_{12}E_5:D_2O:NaI$ . In D), spectrum C) superimposed over the vertical expansion showing that the apparent shoulders are additional peaks.



temperature (25°C) in the magnetic field, the line shape is remarkably affected. The intensity of the outer peaks increases while that of the inner peaks decreases, Fig. 5.11. This behavior is an indication that NaI promotes the formation of the hexagonal phase and the alignment of the domain in the magnetic field.

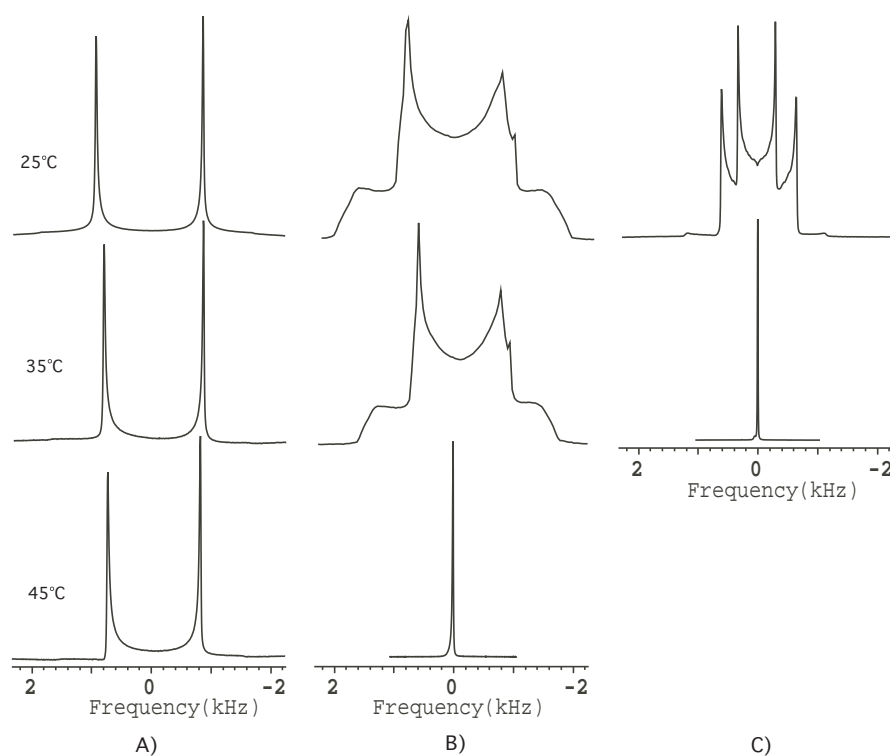


FIGURE 5.13: Deuterium spectra of 70 wt %  $C_{12}E_5$  as a function of the temperature. A)  $C_{12}E_5:D_2O$ . B)  $C_{12}E_5:D_2O:NaCl$ . C)  $C_{12}E_5:D_2O:NaI$

For samples with 70 wt %  $C_{12}E_5$ , the observed spectra exhibit characteristic features representative of the effects of the different salts. We do not need to heat the sample in order to reach the lamellar phase, because they occur already at room temperature. The spectra recorded at 25°C are shown in Fig. 5.12. Consider at the first place the reference spectrum (sample without salts), Fig. 5.12 A). This spectrum is characteristic of the lamellar phases as known from  $^2H$  NMR of  $D_2O$ , and the doublet splitting is 1.74 kHz.

Fig. 5.12 B) shows the spectrum with NaCl as cosolute. The lineshape is totally modified and exhibits a powder-like structure. The peak sep-

aration is 1.513 kHz and the inflection points of shoulders are separated by 3.419 kHz. This structure indicates that the motions take place in an anisotropic environment.

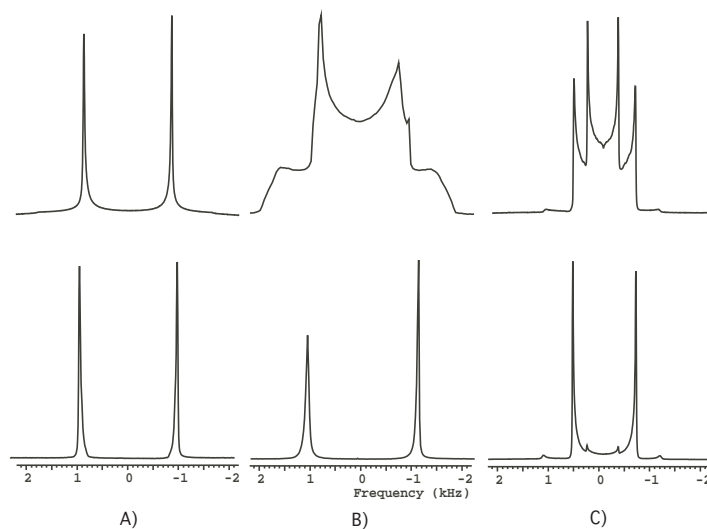


FIGURE 5.14: The spectra at the bottom were recorded after cooling the sample of 70 wt %  $C_{12}E_5$  in the magnetic field. A)  $C_{12}E_5:D_2O$ . B)  $C_{12}E_5:D_2O:NaCl$ . C)  $C_{12}E_5:D_2O:NaI$

In Fig. 5.12 C) we can clearly see that NaI has a profound effect on the structure of the  $L_\alpha$ . The  $^2H$  NMR spectrum consists of two resolved signals with different quadrupolar splittings  $\Delta\nu = 0.609$  kHz and  $\Delta\nu = 1.217$  kHz at 25°C. Moreover, shoulders appear at  $\Delta\nu = 2.243$  kHz. This spectrum indicates a regime of phase coexistence induced by NaI. The signal with a quadrupolar splitting of  $\Delta\nu = 0.609$  kHz might correspond to the hexagonal phase. When we increase the temperature, the phase boundaries are now shifted downward by more than 30°C for NaCl and more than 50°C for NaI, Fig. 5.13.

Following these transformations, if the samples are cooled down in the magnetic field, spectacular changes occur to samples containing salts as shown in Fig. 5.14. The samples are more oriented and the lamellar structure seems to be promoted over the random orientation.

The samples with 80 wt %  $C_{12}E_5$  show a different behavior, Fig. 5.15. In

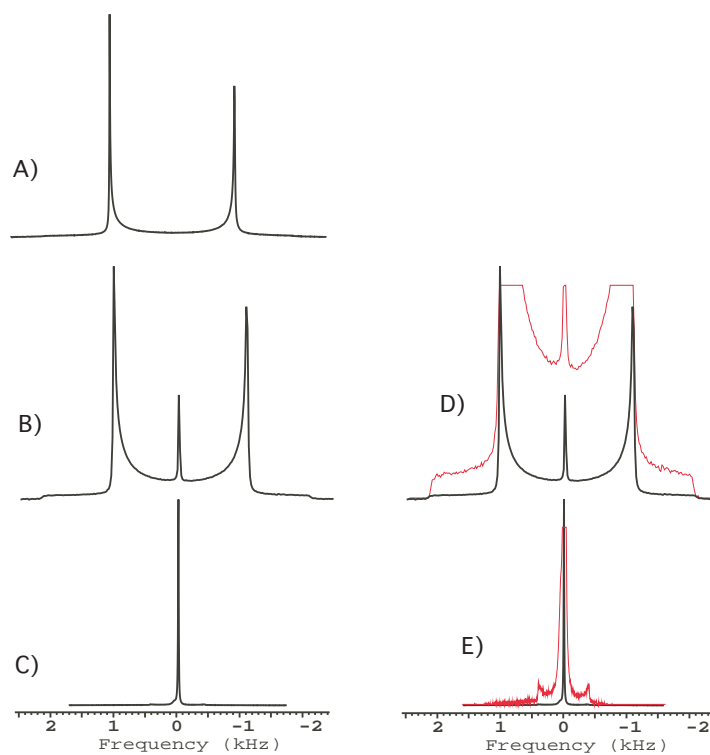


FIGURE 5.15: Deuterium spectra of 80 wt %  $C_{12}E_5$ . A)  $C_{12}E_5:D_2O$ . B)  $C_{12}E_5:D_2O:NaCl$ . C)  $C_{12}E_5:D_2O:NaI$ . In D), spectrum B) superimposed over the vertical expansion showing shoulders. In E), spectrum C) superimposed over the vertical expansion showing that the apparent shoulders are additional peaks.

A) the splitting is obtained as expected for lamellar structures. But in B) we still have a powder-like spectrum in equilibrium with an isotropic phase, that is we have a regime of phase coexistence. Under the effect of NaI, the intensities of the quadrupolar splitting are considerably reduced and only a vertical expansion of the spectrum can show them (Fig. 5.15C) and E)). The boundary of the phase transition are further shifted downward.

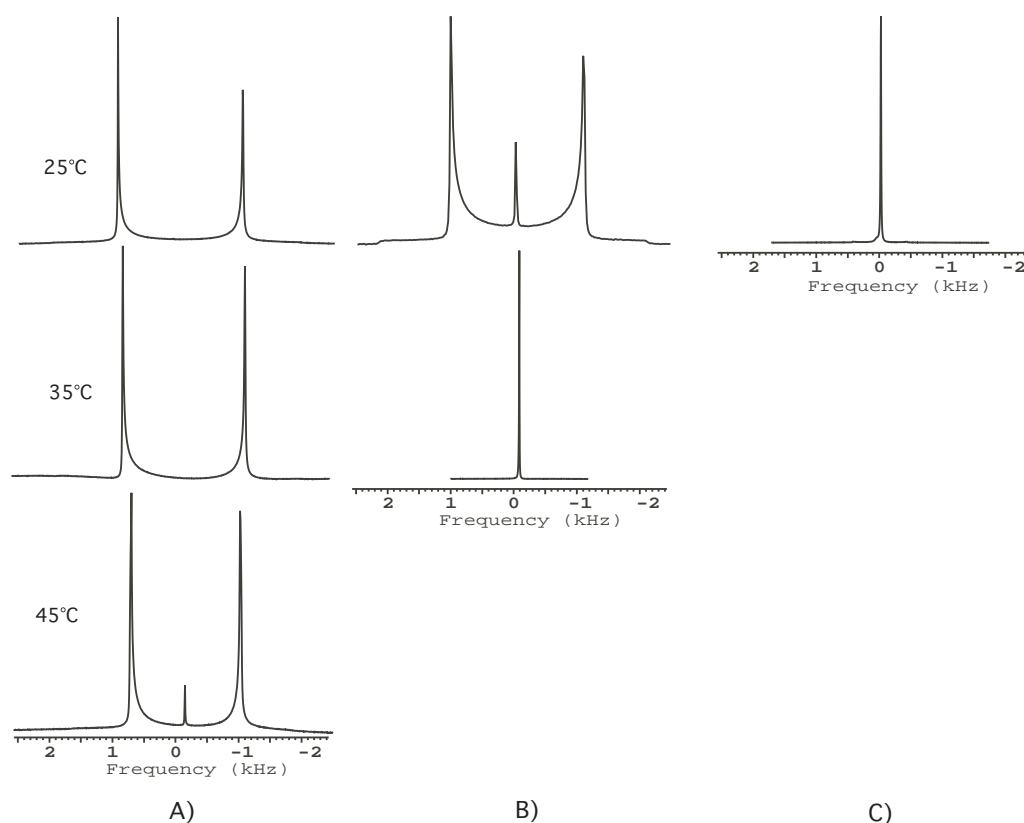


FIGURE 5.16: Deuterium spectra of 80 wt %  $C_{12}E_5$  as a function of the temperature. A)  $C_{12}E_5:D_2O$ . B)  $C_{12}E_5:D_2O:NaCl$ . C)  $C_{12}E_5:D_2O:NaI$

However if the sample with 80 wt %  $C_{12}E_5$  containing the NaI is measured at low temperature ( $22^\circ C$  in this case), we can observe the formation of structure, Fig. 5.17. After the thermal cycle, the spectra show also some structural changes.

To these effects of salt, we can associate a modified phase diagram for the range of temperature and concentration, Fig. 5.18.

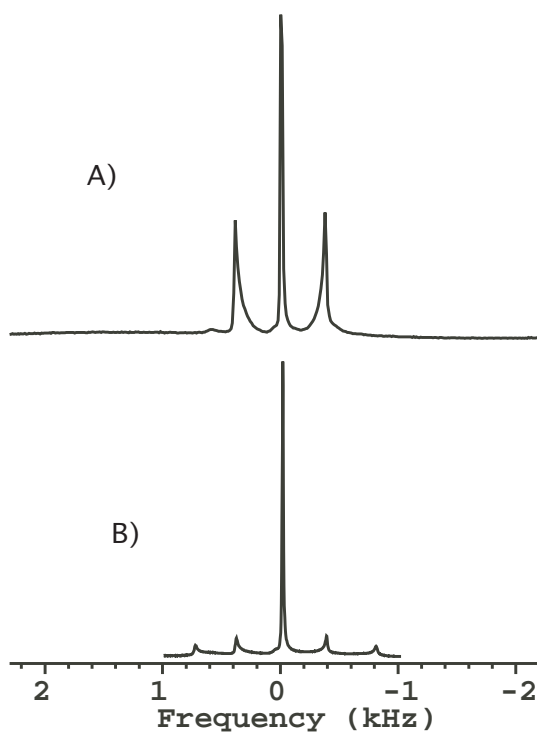


FIGURE 5.17: Shape transformation in the magnetic field (80 wt %  $C_{12}E_5$ ). All the spectra were measured at  $22^\circ\text{C}$ : A) Before heating to the isotropic phase. B) After cooling from the isotropic phase

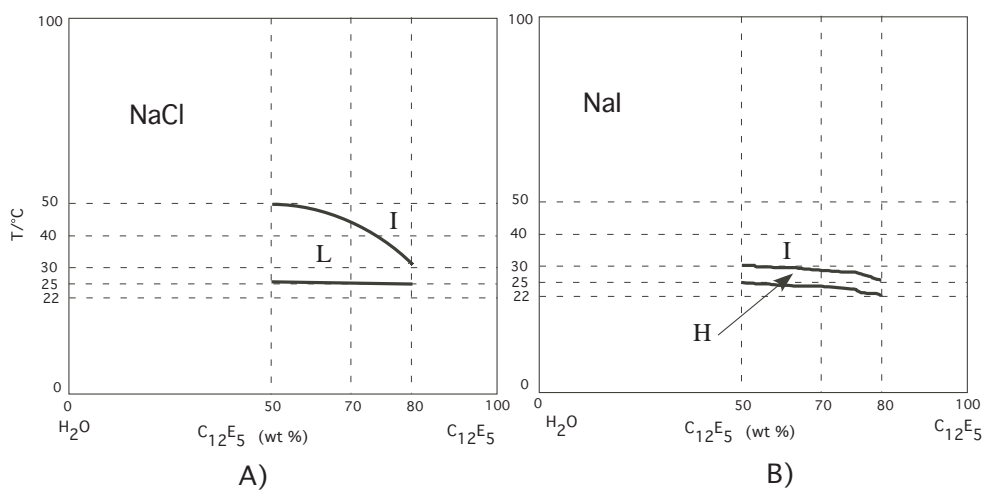


FIGURE 5.18: Modified phase diagram. I, H, L denote the isotropic, hexagonal and lamellar solution respectively. A)  $C_{12}E_5:D_2O:NaCl$ . B)  $C_{12}E_5:D_2O:NaI$

### **And the hydrophobic interaction ?**

Our objective in this study was to determine how the hydrophobic interaction is modified upon addition of salts. But our results show that the lineshape analysis might not be enough to draw reliable conclusions.

A complete interpretation of the data in terms of self-association involves the use of some sort of model which relate the attractive or repulsive interaction between the surfactant molecules. However, considering our results, our intuition indicates that:

- NaCl might promote the formation of aggregates, since the splittings remain within a wide temperature range,
- NaI might decrease the self-association tendency since the structure is destroyed very fast in the range of the observed temperatures.

## **5.6 Conclusion**

An understanding of the effect that salt has on membranes is going to depend on identifying the site of interaction. Are the salts dissolved within the hydrocarbon core of the lipid membranes or are they confined between the bilayers? In our study, we held the ratio surfactant/salt constant (equal to 1 or 0.5 depending on the solubility of the salts), and varied only the ratio surfactant/water (50%, 70% and 80% C<sub>12</sub>E<sub>5</sub>). Changing the water concentration means re-arrangement of water molecules inducing changes in the hydrogen bond network with the consequences that are known [1,48,98]. So the observed changes might be attributed to the change in water contents. Other difficulties in interpreting these types of experiments is that, both the solvent and the bilayer are affected by the presence of salts. However, the temperature shift either upward or downward was already observed while studying the effect of salts on chromonic liquid crystals<sup>2</sup> [100]. An important role was attributed to the cations. A systematic study of the effect of salts at

---

<sup>2</sup>Chromonic liquid crystal are formed by addition of aromatic molecules to water

fixed surfactant/water ratio and at different salt concentrations might supply complementary information regarding the structural changes.

## CHAPTER 6

---

# Conclusion

---

In this study, we have shown how salts influence the various properties of aqueous solutions including the self-association behavior or hydrophobic contacts. The use of NMR to measure the degree of association or the  $A$ -parameter for the system TBA:D<sub>2</sub>O:NaCl, TBA:D<sub>2</sub>O:NaBr and TBA:D<sub>2</sub>O:NaI indicates that NaCl and NaBr show similar influence on the TBA-TBA interaction, that is the tendency of promoting the self-association of TBA molecules in solution, although the effect of NaCl is more pronounced. The result for NaCl was confirmed by molecular dynamics simulation. The anion (Cl<sup>-</sup>) is believed to play an important role, but this role is still discussed, particularly, neutron scattering measurement indicates that a chloride ion bridges two TBA molecules while the molecular dynamics shows no evidence of such bridges. Our result indicates also that NaI induces an opposite effect by preventing the hydrophobic contacts.

We have also shown that salts can induce dramatic changes to the phase behavior of surfactants. Depending on the water content (or the surfactant



content), the salts can shift the temperature of the phase boundaries either upwards or downwards. Only a systematic study of the salt effects at fixed surfactant/water ratio can separate partially the contribution of salts to that of water and indicate which ions (anion or cation) participate in aggregate formation/destruction, although some studies on chromonics liquid crystals point out the role of the cations.

---

## Bibliography

---

- [1] W. Kauzmann. Some factors in the interpretation of protein denaturation. *Adv. Protein Chem.*, 14:1–63, 1959.
- [2] Michael H. Abraham. Free Energies of Solution of Rare Gases and Alkanes in Water and Nonaqueous Solvents. A quantitative assessment of the Hydrophobic Effect. *J. Am. Chem. Soc.*, 101:5477–5484, 1979.
- [3] Charles Tanford. *The Hydrophobic Effect: Formation of Micelles and Biological Membranes*. Krieger Publishing Company, 1991.
- [4] B. Widom, P. Bhimalapuram, and K. Koga. The hydrophobic effect. *Phys. Chem. Chem. Phys.*, 5:3085–3093, 2003.
- [5] Phil Attard. Long-Range Attraction between Hydrophobic Surfaces. *J. Phys. Chem.*, 93:6441–6444, 1989.
- [6] Jan Christer Eriksson, Stig Ljunggren, and Per M. Claesson. A Phenomenological Theory of Long-range Hydrophobic Attraction Forces based on a Squared-gradient Variational Approach. *J. Chem. Soc., Faraday Trans. 2*, 85:163–176, 1989.

- [7] Ka Lum, David Chandler, and John D. Weeks. Hydrophobicity at Small and large Length Scales. *J. Phys. Chem. B*, 103:4570–4577, 1999.
- [8] Phil Attard. Thermodynamic Analysis of Bridging Bubbles and a Quantitative Comparison with the Measured Hydrophobic Attraction. *Langmuir*, 16:4455–4466, 2000.
- [9] S. J. Singer and G. L. Nicolson. The fluid mosaic model of the structure of cell membranes. *Science*, 175:720–731, 1972.
- [10] M. G. Cacace, E. M. landau, and J. J. Ramsden. The Hofmeister series: salt and solvent effects on interfacial phenomena. *Q. Rev. Biophys.*, 30:241–277, 1997.
- [11] Manghaiko Mayele, Manfred Holz, and Antonio Sacco. NMR studies on hydrophobic interactions in solution. Part 4: Temperature and concentration dependence of the hydrophobic self-association of tert-butanol in water. *Phys. Chem. Chem. Phys.*, 1:4615–4618, 1999.
- [12] D.T. Bowron and J. L. Finney. Anion Bridges Drive Salting Out of a Simple Amphiphile from Aqueous Solution. *Phys. Rev. Lett.*, 89:215508–1, 2002.
- [13] Manghaiko Mayele and Manfred Holz. NMR studies on hydrophobic interactions in solution Part 5: Effect of urea on the hydrophobic self-association of tert-butanol in water at different temperatures. *Phys. Chem. Chem. Phys.*, 2:2429–2434, 2000.
- [14] Rainer A. Böckman, Agnieszka Hac, Thomas Heimburg, and Helmut Grubmüller. Effect of Sodium Chloride on a Lipid Bilayer. *Biophys. J.*, 85:1647–1655, 2003.
- [15] Arkadiusz Kozubek, Jerzy Gubernator, Ewa Przeworska, and Maria Stasiuk. Liposomal drug delivery, a novel approach: PLARosomes. *Acta Biochim. Polon.*, 47:639–649, 2000.

- [16] J. S. Beck, J. C. Vartuli, W. J. Roth, M. E. Leonowicz, C. T. Kresge, K. D. Schmitt, C. T-W Chu, D. H. Olson, E. W. Sheppard, S. B. McCullen, J. B. Higgins, and J. L. Schlenker. A New Family of Mesoporous Molecular Sieves Prepared with Liquid crystal Templates. *J. Am. Chem. Soc.*, 114:10834–10843, 1992.
- [17] E. M. Purcell, H. C. Torrey, and R. V. Pound. Resonance Absorption by Nuclear Magnetic Moments in a Solid. *Phys. Rev.*, 69:37–38, 1946.
- [18] F. Bloch, W. W. Hansen, and Martin Packard. Nuclear Induction. *Phys. Rev.*, 69:127, 1946.
- [19] E. Fukushima and S. B. W. Roeder. *Experimental Pulse NMR. A Nuts and Bolts Approach*. Addison-Wesley, 1981.
- [20] Malcom H. Levitt. *Spin Dynamics: Basics of Nuclear Magnetic Resonance*. Wiley, 2001.
- [21] A. Abragam. *The Principles of Nuclear Magnetism*. Oxford University Press, 1961.
- [22] C. P. Slichter. *Principles of Magnetic Resonance*. Springer-Verlag, 1990.
- [23] Jianming Jin. *Electromagnetic Analysis and Design in Magnetic Resonance Imaging*. CRC Press, 1999.
- [24] Richard R. Ernst, Geoffrey Bodenhausen, and Alexander Wokaun. *Principles of Nuclear Magnetic Resonance in One and Two Dimensions*. Clarendon Press, Oxford, 1987.
- [25] Martin Blackledge. Recent progress in the study of biomolecular structure and dynamics in solution from residual dipolar couplings. *Prog. NMR Spectrosc.*, 46:23–61, 2005.
- [26] J. Seelig. Deuterium Magnetic Resonance: Theory and Application to lipid membranes. *Quarterly Reviews of Biophysics*, 10:353–418, 1977.

- [27] Klaus Schmidt-Rohr and Hans Wolfgang Spiess. *Multidimensional Solid-state NMR and Polymers*. Academic Press, 1994.
- [28] Melinda J. Duer. *Introduction to Solid-State NMR Spectroscopy*. Blackwell Publishing, 2004.
- [29] F. Bloch. Nuclear Induction. *Phys. Rev.*, 70:460–474, 1946.
- [30] R. K. Wangsness and F. Bloch. The Dynamical Theory of Nuclear Induction. *Phys. Rev.*, 89(4):728–739, 1953.
- [31] A. G. Redfield. On the Theory of Relaxation Processes. *IBM Journal of Research and Development*, 1957.
- [32] E.O. Stejskal and J. E. Tanner. Spin Diffusion Measurements: Spin Echoes in the Presence of a Time-Dependent Field Gradient. *J. Chem. Phys.*, 42:288–292, 1965.
- [33] Peter Stilbs. Fourier Transform Pulsed Gradient Spin-echo Studies of Molecular Diffusion. *Prog. NMR Spectrosc.*, 19:1–45, 1987.
- [34] William S. Price. Pulsed-Field Gradient Nuclear Magnetic Resonance as a Tool for Studying Translational Diffusion: Part II. Experimental Aspects. *Concepts Magn. Reson.*, 10:197–237, 1998.
- [35] Paul T. Callaghan and Yang Xia. Velocity and Diffusion imaging in Dynamic NMR Microscopy. *J. Magn. Reson.*, 91:326–352, 1991.
- [36] Hakan Hagslätt, Bengt Jösso, Magnus Nydén, and Olle Söderman. Predictions of pulsed field gradient NMR echo-decays for molecules diffusing in various restrictive geometries. Simulations of diffusion propagators based on a finite element method. *J. Magn. Reson.*, 161:138–147, 2003.
- [37] Göran Lindblom and G. Oradd. NMR Studies of Translational Diffusion in Lyotropic Liquid Crystals and Lipid Membranes. *Prog. NMR Spectrosc.*, 26:483, 1994.

- [38] James S. Murday. Measurement of magnetic Field Gradient by its Effect on the NMR Free Induction Decay. *J. Magn. Reson.*, 10:111–120, 1973.
- [39] M. Holz and H. Weingärtner. Calibration in Accurate Spin-Echo Self-Diffusion Measurements Using  $^1\text{H}$  and Less-Common Nuclei. *J. Magn. Reson.*, 92:115–125, 1991.
- [40] Geoffrey C. Maitland, Maurice Rigby, E. Brian Smith, and William A. Wakeham. *Intermolecular Forces: Their Origin and Determination*. Oxford, 1981.
- [41] Jacob N. Israelachvili. *Intermolecular and Surface Forces: With Applications to Colloidal and Biological Systems*. Academic Press, 1985.
- [42] Drew Myers. *Surfaces, Interfaces, and Colloids*. Wiley-VCH, 1999.
- [43] P. L. Huyskens, W. A. P. Luck, and T. Zeegers-Huyskens, editors. *Intermolecular Forces: an Introduction to Modern Methods and Results*. Springer-Verlag, 1991.
- [44] Hans-Jörg Schneider. Mechanism of Molecular Recognition: Investigations of Organic Host-Guest Complexes. *Angew. Chem. Int. Ed. Engl.*, 30:1417–1436, 1991.
- [45] Arieh Ben-naim. *Hydrophobic Interactions*. Plenum Press, 1980.
- [46] Lawrence R. Pratt. Molecular Theory of Hydrophobic Effects: "She is too mean to have name repeated. *Ann. Rev. Phys. Chem.*, 53:409–436, 2002.
- [47] Pieter Rein ten Wolde. Hydrophobic interactions: an overview. *J. Phys.: Condens. Matter*, 14:9445–9460, 2002.
- [48] David Chandler. Interfaces and the driving force of hydrophobic assembly. *Nature*, 437:640–647, 2005.

- [49] P. M. Wiggins. Role of water in some biological processes. *Microbiol. Rev.*, 54:432–449, 1990.
- [50] John L. Finney. Water? What's so special about it? *Phil. Trans. R. Soc. Lond. B*, 359:1145–1165, 2004.
- [51] Henry S. Frank and Majorie W. Evans. Free Volume and Entropy in Condensed Systems. III Entropy in Binary Mixtures; Partial Molar Entropy in Dilute Solutions; Structure and Thermodynamics in Aqueous Electrolytes. *J. Chem. Phys.*, 13:507–532, 1945.
- [52] George Némethy and Harold A. Scheraga. Structure of Water and Hydrophobic Bonding in Proteins. I. A Model for the Thermodynamic Properties of Liquid Water. *J. Chem. Phys.*, 36:3382–3400, 1962.
- [53] H. J. Bakker, M. F. Kropman, and A. W. Omta. Effect of ions on the structure and dynamics of liquid water. *J. Phys.: Condens. Matter*, 17:S3215–S3224, 2005.
- [54] V. Degiorgio and M. Corti, editors. *Physics of Amphiphiles: Micelles, Vesicles and Microemulsions*. North-Holland, 1985.
- [55] R. Nagarajan. Molecular Packing Parameter and Surfactant Self-Assembly: The Neglected Role of the Surfactant Tail. *Langmuir*, 18:31–38, 2002.
- [56] M. Kinoshita and F. Hirata. Analysis of salt effects on solubility of noble gases in water using the reference interaction site model. *J. Chem. Phys.*, 106:5202–5215, 1997.
- [57] T. Ghosh, A. Kalra, and S. Garde. On the salt-induced stabilization of pair and many-body hydrophobic interactions. *J. Phys. Chem. B*, 109:642–651, 2005.
- [58] Jerry Tsai, Mark Gerstein, and Michael Levitt. Keeping the shape but changing the charges: A simulation study of urea and its iso-steric analogs. *J. Chem. Phys.*, 104:9417–9430, 1996.

- [59] S. Dixit, W. C. K. Poon, and J. Crain. Hydration of methanol in aqueous solutions: a Raman spectroscopic study. *J. Phys. Condens. Matter*, 12:L323–L328, 2000.
- [60] D. T. Bowron, J. L. Finney, and A. K. Soper. The structure of pure tertiary butanol. *Mol. Phys.*, 93:531–543, 1998.
- [61] Peter G. Kusalik, Alexander P. Lyubartsev, Dan L. Bergman, and Aatto Laaksonen. Computer Simulation Study of tert-Butyl Alcohol. 1. Structure in the Pure Liquid. *J. Phys. Chem. B*, 104:9526–9532, 2000.
- [62] D. T. Bowron, J. L. Finney, and A. K. Soper. Structural Investigation of Solute-Solute Interactions in Aqueous Solutions of Tertiary Butanol. *J. Phys. Chem. B*, 102:3551–3563, 1998.
- [63] John L Finney, Daniel T Bowron, and Alan K Soper. The structure of aqueous solutions of tertiary butanol. *J. Phys.: Condens. Matter*, 12:A123–A128, 2000.
- [64] A. K. Soper and J. L. Finney. Hydration of Methanol in Aqueous Solution. *Phys. Rev. Lett.*, 71(26):4346–4350, 1993.
- [65] Peter G. Kusalik, Alexander P. Lyubartsev, Dan L. Bergman, and Aatto Laaksonen. Computer Simulation Study of tert-Butyl Alcohol. 2. Structure in Aqueous Solution. *J. Phys. Chem. B*, 104:9533–9539, 2000.
- [66] S. Dixit, J. Crain, W. C. K. Poon, J. L. Finney, and A. K. Soper. Molecular segregation observed in a concentrated alcohol-water solution. *Nature*, 416:829–832, 2002.
- [67] J.-H. Guo, Y. Luo, A. Augustsson, Kashtanov, J.-E. Rubensson, D. K. Shuh, H. Agren, and J. Nordgren. Molecular Structure of Alcohol-Water Mixtures. *Phys. Rev. Lett.*, 91:157401–1, 2003.
- [68] Antonio Sacco and Manfred Holz. NMR studies on hydrophobic interactions in solution Part 2. temperature and urea effect on the self-



- association of ethanol in water. *J. Chem. Soc., Faraday T rans.*, 93:1101–1104, 1997.
- [69] Antonio Sacco, Francesca Maria De Cillis, and Manfred Holz. NMR studies on hydrophobic interactions in solution Part 3: Salt effects on the self-association of ethanol in water at two different temperatures. *J. Chem. Soc., Faraday T rans.*, 94:2089–2092, 1998.
- [70] D. T. Bowron and J. L. Finney. Structure of a salt-amphiphile-water solution and the mechanism of salting out. *J. Chem. Phys.*, 118:8357–8372, 2003.
- [71] N. Bloembergen, E. M. Purcel, and R. V. Pound. Relaxation effects in nuclear magnetic resonance absorption. *Phys. Rev.*, 73(7):679–715, 1948.
- [72] P. Westlund and R. Lynden-Bell. A molecular dynamics study of the intermolecular spin-spin dipole-dipole correlation function of liquid acetonitrile. *J. Magn. Reson.*, 72:522–531, 1987.
- [73] E. O. Stejksal, D. E. Woessner, T. C. Farrar, and H. S. Gutowsky. Proton Magnetic Resonance of the CH<sub>3</sub> Group. V. Temperature Dependence of  $T_1$  in Several Molecular Crystals. *J. Chem. Phys.*, 31:55–65, 1959.
- [74] H. G. Hertz and C. Radle. The Orientation of the Water Molecules in the Hydration Sphere of F<sup>-</sup> and in the Hydrophobic Hydration Sphere. *Ber. Bunsenges. physik. Chem.*, 77(7):521–531, 1973.
- [75] H. G. Hertz. Information on the Orientation Dependant Molecular Distribution Function from Nuclear Magnetic Relaxation Data. *Ber. Bunsenges. physik. Chem.*, 80(10):950–957, 1976.
- [76] M. Odelius, A. Laaksonen, M. H. Levitt, and J. Kowalewski. Intermolecular Dipole-Dipole Relaxation. A Molecular Dynamics Simulation. *J. Magn. Reson. A*, 105:289–294, 1993.

- [77] H. G. Hertz. Microdynamic Behaviour of Liquids as studied by NMR Relaxation Times. *Prog. NMR Spec.*, 3(159):159–230, 1967.
- [78] H. G. Hertz and R. Tutsch. Model Orientation Dependent Pair Distribution Functions Describing the Association of Simple Carboxylic Acids and of Ethanol in Aqueous Solution. *Ber. Bunsenges. physik. Chem.*, 80:1268–1278, 1976.
- [79] P. A. Egelstaff. *An Introduction to the Liquid State*. Oxford, 1994.
- [80] A. L. Capparelli, H. G. Hertz, and R. Tutsch. An Investigation of the Structure of the Mixture Acetic Acid-Cyclohexane by the Nuclear Magnetic Relaxation Method. *J. Phys. Chem.*, 82(18):2023–2029, 1978.
- [81] K. J. Muller and H. G. Hertz. A Parameter as an Indicator for Water-Water Association in Solution of Strong Electrolytes. *J. Phys. Chem.*, 100:1256–1265, 1996.
- [82] Ulrike Wandle and H. G. Hertz. Sharpening of the OH...OH Pair Correlation Function when Liquid Methanol is Diluted in CCl<sub>4</sub>. *Z. Phys. Chem.*, 178:217–228, 1992.
- [83] Dietmar Paschek, Alfons Geiger, Momo Jeufack Hervé, and Dieter Suter. Adding salt to an aqueous solution of t-butanol: Do we observe an enhanced or a reduced hydrophobic association? submitted, July 2005.
- [84] M. Sass and D. Ziessow. Error Analysis for Optimized Inversion Recovery Spin-Lattice Relaxation Measurements. *J. Magn. Reson.*, 25:263–276, 1977.
- [85] Jeffrey L. Evelhoch and Joseph J. H. Ackerman. NMR T<sub>1</sub> measurements in inhomogeneous B<sub>1</sub> with surface coils. *J. Magn. Reson.*, 53:52–64, 1983.

- [86] L. R. Whalley and C. E. Tarr. A Three-Parameter Non-linear Procedure for Fitting Inversion-Recovery Measurement of Spin-Lattice Relaxation Times. *J. Magn. Reson.*, 26:533–536, 1977.
- [87] G. Bonera and A. Rigamonti. Intra- and Intermolecular Contributions to the Proton Spin-Lattice Relaxation in Liquids. *J. Chem. Phys.*, 42(1):171–174, 1965.
- [88] Alexander G. Petrov. *The Lyotropic State of Matter*. Gordon and Breach, 1999.
- [89] E. Sackmann. Dynamic Molecular Organization in Vesicles and Membranes. *Ber. Bunsenges. physik. Chem.*, 82:891–909, 1978.
- [90] Russel E. Jacobs and Eric Oldfield. NMR of Membranes. *Prog. NMR Spectrosc.*, 14:113–136, 1981.
- [91] Shri Singh. *Liquid Crystals: Fundamentals*. World Scientific, 2002.
- [92] Charles R. I. Sanders, Brian Hare, Kathleen P. Howard, and James H. Prestegard. Magnetically-oriented phospholipid micelles as tool for the study of membrane associated molecules. *Prog. NMR Spectrosc.*, 26:421–444, 1994.
- [93] Aksel A. Bothner-By. Magnetic Field Induced Alignment of Molecules. *Encyclopedia of NMR*, 5:2932–2938, 1996.
- [94] A. Firouzi, D. J. Schaefer, S. H. Tolbert, G. D. Stucky, and B. F. Chmelka. Magnetic-Field-Induced Orientational Ordering of Alkaline Lyotropic Silicate-Surfactant Liquid Crystals. *J. Am. Chem. Soc.*, 119:9466–9477, 1997.
- [95] Hugo Christenson and Stig E. Friberg. Spectroscopic Investigation of the Mutual Interactions between Nonionic Surfactant, Hydrocarbon, and water. *J. Colloid Interface Sci.*, 75:276–285, 1979.

- [96] Reinhard Strey, Reinhard Schomäcker, Didier Roux, Frederic Nallet, and Ulf Olsson. Dilute Lamellar and L3 Phases in the Binary Water- $C_{12}E_5$  System. *J. Chem. Soc., Faraday Trans.*, 86:2253–2261, 1990.
- [97] C. Stubenrauch, S. Burauer, and R. Strey. A new approach to lamellar phases ( $L_\alpha$ ) in water ? non-ionic surfactant systems. *Liq. Cryst.*, 31:39–53, 2004.
- [98] Akimitsu Tonegawa, Keiichi Ohno, Hiroatsu Matsuura, Koji Yamada, and Tsutomu Okuda. A Combined Raman and Deuterium NMR Study on the Molecular and Phase Structure of a Nonionic Surfactant C12E5-Water system. *J. Phys. Chem. B*, 106:13211–13223, 2002.
- [99] Giuseppe Briganti, Anna L. Segre, Donatella Capitani, Cinzia Casieri, and Camillo La Mesa. Isooriented Lyotropic Lamellar Phase in the C12E6/D2O System. *J. Phys. Chem. B*, 103:825–830, 1999.
- [100] Andrei F. Kostko, Bani H. Cipriano, Olga A. Pinchuk, Lior Ziserman, Mikhail A. Anisimov, Dganit Danino, and Srinivasa R. Raghavan. Salts Effects on the Phase Behavior, Structure, and Rheology of Chromonic Liquid Crystals. *J. Chem. Phys. B*, 109:19126–19133, 2005.

---

# Acknowledgements

---

This thesis is the result of 56 months of work whereby I have been accompanied and supported by many people. Today, I am very pleased to express my gratitude for all of them.

The first person I would like to thank is my supervisor Prof. Dr. Dieter Suter. His integral view on research and his mission for providing high-quality work has made a deep impression on me. I owe him lots of gratitude for having me shown this way of research. He would never realized how much I learned from him.

I would like to thank Dr. Reiner K uchler who helps me to carry out my first NMR experiment and who was always available when I need his advises.

I would also like to thank the member of my Ph.D committee who monitored my work and took effort in reading and providing me with valuable comment on earlier versions of this thesis.

Of course I should not forget to mention my colleagues H. G. Krojanski, S. Markowa, K. W. Lim and all the E III people for their help in various expect. I would like to further express my thanks to Mr. H. Romberck and Mrs A. Sommer for invaluable help and support concerning the administrative

formalities.

I wish to extend my thanks to Dr. D. Paschek and Prof. A. Geiger for the fruitful collaboration.

The financial support of the University of Dortmund and the Graduierten Kolleg "Struktur-Dynamik-Beziehungen in mikrostrukturierten Systemen" is gratefully acknowledged.

I feel a deep sense of gratitude to my family (I missed you a lot!!) for constantly cheering me up and for untiring encouragements, to my family in-laws which also encourage me a lot.

I would like to give my special thanks to my fiancée Arlette R. Theinkeu N. for her love and patience during the Ph.D period.

The chain of my gratitude would be definitely incomplete if I would forget to thank my neighbor Hans Jurgen Poggendorf and Adyeri N, who were always willing to help, and also I would like to thank all my friends for the mutual motivation, for the mutual encouragement and for nice time that we had sometime together.

Dortmund, January 2006

Momo Jeufack Hervé